Parametric Study of Hypoplasticity Constitutive Model for Granular Media via the Discrete Element Method

Yufei Zhou
Marquette University

PARAMETRIC STUDY OF HYPOPLASTICITY CONSTITUTIVE MODEL FOR GRANULAR MEDIA VIA THE DISCRETE ELEMENT METHOD

by

Yufei Zhou, B.S.M.E

A Thesis submitted to the Faculty of the Graduate School,
Marquette University,
in Partial Fulfillment of the Requirements for
the Degree of Master of Science

Milwaukee, Wisconsin

May 2019

ABSTRACT

Parametric study of Hypoplasticity Constitutive Model for Granular Media via the Discrete Element Method

Yufei Zhou, B.S.M.E

Marquette University, 2018

Granular media, as a general definition, includes a large class of materials, such as cereal grains; pharmaceutical tablets and capsules; geomaterials, such as sand; and the masses of rock and ice in planetary rings. Alternatively, a granular material could consist of highly fractured rock masses regarded as cracked elastic solids. In all cases, a very important property of granular media is their ability to yield, that is, exhibit irreversible deformation properties. Because the granular elastic modulus 'G' is the key relevant stress parameter, there is an interesting and nagging question as to the microscopic origins of the stress scales assumed in various empiricisms associated with critical-state soil mechanics and Hypoplasticity. This question may reflect a philosophical divide, separating those concerned with the relation of constitutive equations to micromechanics, from those whose primary concern is correlation of data from laboratory and field tests.

The goal of this research is to first understand how hypoplastic constitutive equation works to account for the granular material behavior. From the original Hypoplastic constitutive equation which was introduced by Kolymbas, Lade-Duncan, Mohr-Coulomb and Matsuoka-Nakai yield surfaces (which are regarded as the significant approach for yield prediction in elastoplasticity theory) are generated. Then, with the Discrete Element Method (DEM) true triaxial test results, the parametric study is processed by the developed inverse hypoplastic constitutive equation.

The results show the concept of inverting the hypoplastic constitutive model is capable of generating the actual and effective non-dimensional material parameters. Due to the input of the improved stress and strain obtained from the true-triaxial test, the improved method is shown to be improved from original experimental data. Also, the Hypoplastic method performs as effective as the other previous method such as elastoplastic.

TABLE OF CONTENTS

LIST OF FIGURES ……... iii

NOMENCLATURE …….. vi

1 INTRODUCTION ...……... 1

1.1 Problem Summary ……..……..... 2

1.2 Literature Review …….. 3

1.2.1 Constitutive Equation …….…… 3

1.2.2 Early theory to describe the behavior of granular media (e.g. soil)..3

1.2.3 Hypoplasticity ……... 5

1.2.4 Summary …….……... 7

1.3 Objectives and Methodology ……...……. 7

2 THEORETICAL BACKGROUND ……...… 10

2.1 Fundamentals of Continuum Mechanics ….…….. 10

2.2 Hypoplasticity Background …….……13

2.2.1 Rate Equation……13

2.2.2 Restriction on the Constitutive Equation……...……15

2.3 Yield Surface……16

3 EXPERIMENTAL SET UP…… 18

3.1 Yield Surface in Elasto-plasticity ……...…… 18

3.1.1 Material Strength Parameters …… 18

3.1.2 Calibration ……...…… 20

3.2 Hypoplastic Model Description …… 22

3.3 Hypoplastic Constitutive Model ……. 24

3.3.1 General Model ……. 24

3.3.2 Limit States of Hypoplasticity ……..…. 24

3.3.3 Specific Model ……. 26

3.3.4 Improved Yield Surface with Hypoplasticity ……...… 28

4 PARAMETER STUDY WITH DEM TRUE-TRIAXIAL TEST……... 39

4.1 DEM true-triaxial test ……. 40

4.2 Parameter of hypoplastic constitutive model study ……..... 43

5 RESULT AND DISCUSSION …….. 50

5.1 3000-30000 mono-disperse spheres ……..….. 50

5.2 125000 spherical poly-disperse spheres …….……...….. 68

6 CONCLUSIONS AND FUTURE WORK……..….... 77

6.1 Conclusion……..……...….. 77

6.2 Future work……..……..….. 78

BIBLIOGRAPHY……..……...…… 80

LIST OF FIGURES

Figure 1-1. Loading, unloading and reloading…… 4

Figure 2-1. x is the position vector at time t for the particle P, and X is the position at time t_0 …..…….... 11

Figure 2-2. (a)(b) (a). Yield surface viewed as cones in principal stress space and (b). intersection of Mohr-Coulomb, Drucker-Prager, Matsuoka-Nakai and Lade-Duncan yield surfaces with the π-plane ……..…….…… 17

Figure 3-1. Calibrated four yield surfaces through Elasto-plastic Method……..... 21

Figure 3-2. Stress History by Hypoplasticity Model with initial condition …….. 27

Figure 3-3. Partial yield cone formed by the stress paths corresponding to the true-triaxial test for the DEM simulation in [10] ……..…. 27

Figure 3-4. Hypoplasticity yield surface in terms of $C_i, i = 1,2,3,4$ in Table 3-3, matching with Drucker-Prager, Matsuoka-Nakai and Lade-Duncan yield surface in elasto-plasticity ……29

Figure 3-5. Sixteen cases (Δ=20) calibrated with Hypoplastic model in [9], Drucker-Prager, Matsuoka-Nakai and Lade-Duncan yield surface in elasto-plasticity ……... 31

Figure 3-6. illustration of sixteen cases on the π-plane ……..… 32
Figure 3-7. illustration of sixteen cases on the π-plane ……. 33

Figure 3-8. illustration of sixteen cases on the π-plane ……. 35

Figure 3-9. Hypoplastic Lade-Duncan and Hypoplastic Matsuoka-Nakai yield surface matched with original Drucker-Prager, Lade-Duncan and Matsuoka-Nakai yield surface……... 37

Figure 4-1. Three dimensional micromechanical effects involving inter-particle contact and motion on macro-scale slip plane ……..…… 40

Figure 4-2. 125000-sphere cubical DEM specimen for true-triaxial test simulation …..... 42

Figure 5-1. The parameter C for specimen 4 under μ = 0.2, 0.5, 0.8 with each plastic case ……... 51

Figure 5-2. The parameter C for specimen 5 under μ = 0.2, 0.5, 0.8 with each plastic case ……... 52

Figure 5-3. The parameter C for specimen 6 under μ = 0.2, 0.5, 0.8 with each plastic case ……..…. 53

Figure 5-4. Stress path for Specimen 4 contained the DEM original, stress paths with each time step parameter C, re-substituted hypoplastic and well-matched constant C value 54

Figure 5-5. Stress path for Specimen 5 contained the DEM original, stress paths with each time step parameter C, re-substituted hypoplastic and well-matched constant C value … 56

Figure 5-6. Stress path for Specimen 5 with $\mu = 0.5$ & 0.8 (plastic 9) ……. 57

Figure 5-7. Stress path for Specimen 6 contained the DEM original, stress paths with each time step parameter C, re-substituted hypoplastic and well-matched constant C value … 58

Figure 5-8. Stress paths for specimen 4 where (a) $\mu = 0.2$ plastic 9 (b) $\mu = 0.2$ plastic 11 (c) $\mu = 0.2$ plastic 12 (d) $\mu = 0.5$ plastic 14 (e) $\mu = 0.8$ plastic 11 …..……..… 59

Figure 5-9. Stress paths for specimen 5 where (a) $\mu = 0.2$ plastic 9 (b) $\mu = 0.5$ plastic 10 (c) $\mu = 0.8$ plastic 10 (d) $\mu = 0.8$ plastic 11 ……..……. 61

Figure 5-10. Stress paths for specimen 5 where (a) $\mu = 0.2$ plastic 9 (b) $\mu = 0.2$ plastic 10 (c) $\mu = 0.8$ plastic 14 ……...……...…... 62

Figure 5-11. Hypoplastic yield surface in terms of specimen 4 with different non-dimensional material parameters $C_i, i = 1,2,3,4$ ……...……... 63

Figure 5-12. Hypoplastic yield surface in terms of specimen 5 with different non-dimensional material parameters $C_i, i = 1,2,3,4$ ……...……...… 65

Figure 5-13. Hypoplastic yield surface in terms of specimen 6 with different non-dimensional material parameters $C_i, i = 1,2,3,4$ ……...……...… 67

Figure 5-14. The parameter C for 125000 spherical poly-disperse spheres ……..…. 70

Figure 5-15. The parameter C for 125000 spherical poly-disperse spheres both smoothed (solid line) and the original (dotted line) ……..……..... 71

Figure 5-16. Hypoplastic yield surface in terms of original DEM true-triaxial test data for 125000 spherical poly-disperse spheres with different non-dimensional material parameters $C_i, i = 1,2,3,4$ under seven lode angle α condition ……...…. 72

Figure 5-17. Hypoplastic yield surface in terms of smoothed DEM true-triaxial test data for 125000 spherical poly-disperse spheres with different non-dimensional material parameters $C_i, i = 1,2,3,4$ under seven lode angle α condition ……. 74

NOMENCLATURE

B	second order tensor rewritten from Hypoplastic constitutive equation
C_i	material constants for specific granular material, where *i = 1,2,3,4.*
D	EULER's stretching (strain rate) tensor
F	the deformation gradient tensor
R	orthogonal rotation tensor
T	stress tensor
T^*	deviatoric stress tensor
$\dot{T}$	stress rate tensor
$\ddot{T}$	JAUMANN stress tensor
U	right stretch tensor
V	left stretch tensor
W	CAUCHY's spin tensor
x_i	position with the spatial (or EULER) coordinates, where *i = 1,2,3.*
X_j	position with the material (or LAGRANGE) coordinates, where *j = 1,2,3.*
α	Lode angle
φ	friction angle

1 Introduction

Granular media, as a general definition, includes a large class of materials, such as cereal grains; pharmaceutical tablets and capsules; geomaterials, such as sand; and the masses of rock and ice in planetary rings. [1] Alternatively, a granular material could consist of highly fractured rock masses regarded as cracked elastic solids. [2] And the elastic behavior will vanish in a critical state. In all cases, a very important property of granular media is their ability to yield. And in the theory of elastoplasticity the condition in terms of stress state is called the yield surface. [1]

The current research on granular mechanics as the phenomenological continuum models is mainly concerned with dry granular materials, or else with those completely saturated by an interstitial fluid, in which capillary forces and other forms of cohesion are largely negligible. Hence, the above restrictions rule out applications to the fine powders, colloidal systems, and clayey soils discussed in other works [3,4]. Because of the granular elastic modulus 'G' is the only relevant stress scale, there is an interesting and nagging question as to the microscopic origins of the stress scales assumed in various empiricisms associated with critical-state soil mechanics and hypoplasticity (e.g., [4-8]). This question may reflect a philosophical divide, separating those concerned with the relation of constitutive equations to micromechanics from those whose primary concern is correlation of data from laboratory and field tests ([6], p. 13). [1]

As a mathematical method connecting stress and strain for a specific material, the constitutive equation is introduced. It is important to predict the stability of a slope or to predict the deformation around an excavation etc. with using the constitutive equation of soil. As for soil with continued loading, an elastoplasticity constitutive equation is released

to determine the initial elastic deformation whereas the plastic deformation later. But do the elastoplasticity constitutive equation is the best or the only way to depict the soil behavior? The present work evaluates, through different numerical simulation and theoretical analysis, hypoplastic constitutive equation is the better model which avoid the shortcoming with the elastoplastical method (the detail will be mentioned later).

In this thesis, a hypoplastic constitutive equation which aims to describe the anelastic phenomena without using extra notions introduced by elastoplasticity is introduced to match results of the true-triaxial test simulation. [10]

The remainder of this thesis is as follows. Chapter1, Chapter2, Chapter3

1.1 Problem Summary

Regarding the hypoplasticity, many studies have been performed previously to validate its effect on granular mechanics. Kolymbas introduced an incrementally nonlinear constitutive equation for soils which was generalized by hypoelasticity in 1977. As the prototype of hypoplastic constitutive equation, this model already included the main ingredient of hypoplasticity, i.e. incremental nonlinearity by the norm of the strain rate. [11] After that various kinds of hypoplastic constitutive equation was proposed with main concept, i.e. the constitutive equation was separated to two parts, linear part and nonlinear part. The research for this thesis will perform studies on the advanced models from [9] and test them to understand the connection between the hypoplasticity and hypoelasticity.

Another problem is also addressed in this research. As significant approach was achieved by Dr. Fleishman, the yield criterion has proven itself to be a main method for predicting the continuum-based failure of non-cohesive granular materials (soils in this thesis) with elastoplasticity theory. There are several yield criterions i.e. Lade-Duncan,

Matsuoka-Nakai, Mohr-Coulomb, Drucker-Prager etc. From them, the Lade-Duncan yield surface has been validated as the best one in recent decades by hundreds of numerical simulations of true-triaxial tests performed using the Discrete Element Method (DEM). [10] Since its great job in elastoplasticity, it will be fun to get the Lade-Duncan yield surface in hypoplasticity with the data from the numerical simulations of true-triaxial tests. At the same time, other kinds of yield surfaces i.e. Matsuoka-Nakai, Mohr-Coulomb, Drucker-Prager etc. will be generated.

1.2 Literature Review

1.2.1 Constitutive Equation

As a great mathematical relation connecting stress and strain for a particular material, a constitutive equation helps to understand the behavior of this material. The stress and strain are tensorial quantities here. There are also some additional quantities, the material constants such as the YOUNG's modulus in a constitutive model. The value of the material constants depends on the specific material, i.e. they make possible to distinguish e.g. between an elastic rubber and an elastic steel. [9] Here, a question is raised, i.e. 'what for is a constitutive equation useful?'. The soil's constitutive equation is needed to predict the stability of a slope or a cut, or to predict the loads applied on the lining of a basement or a tunnel. Previously, we use the balance laws of mechanics (balance of mass and momentum) to answer these aforementioned questions. But it is insufficient to solve the problem with the balance laws. In order to collect more additional needed information, the constitutive equation become extremely necessary.

1.2.2 Early theory to describe the behavior of granular media (e.g. soil)

The property of elasticity is given if the stress (or strain) depends on the strain (or stress). As the definition of the path-independence, it means that the strain (or stress) history is immaterial and only the actual value of stress (or strain). In other word, the previous history can be conceived as a strain- (or stress-) path. Another version is that elasticity means that the stress is a function of strain (or the strain is a function of stress). And the elastic materials do not show the irreversible deformation after unloading. However, as we all know that if we walk on a sandy beach we leave trace behind. And in some materials, such as steel, plastic deformations are only occurred if the stress exceeds a particular limit. [9] Hence it is inappropriate to describe the behavior of soil only with the theory of elasticity. A cycle of loading and unloading leaves always an irreversible or plastic deformation behind (figure1-1).

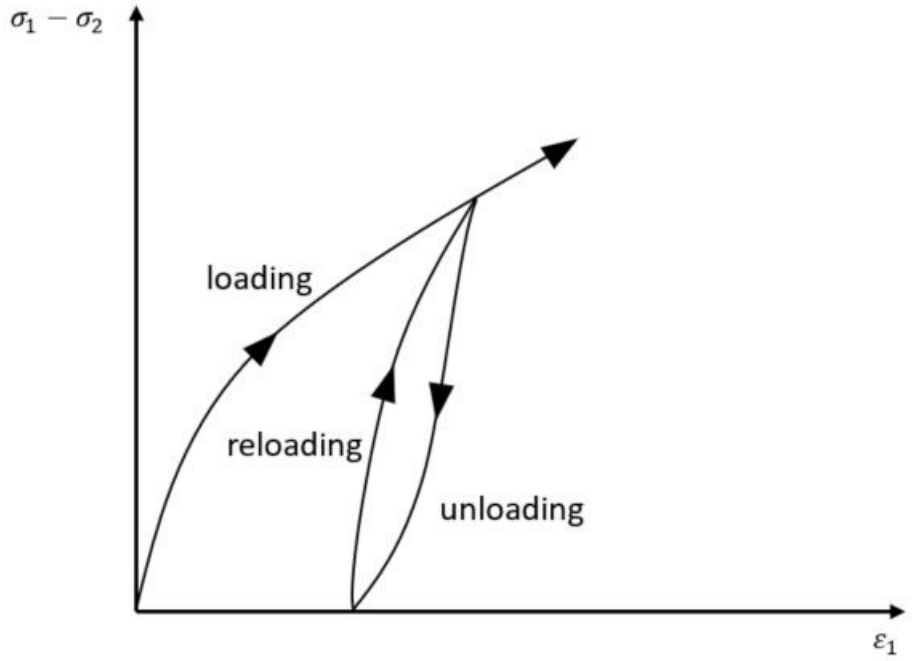

Figure 1-1 loading, unloading and reloading

Then, a question was raised that ‘how to describe anelastic deformations?’. It is integrant to provide different stiffnesses for loading and unloading in a constitutive equation. Here, a widespread mathematical framework for aforementioned irreversible deformations is introduced, so-called elastoplasticity. According to elastoplasticity, a material behaves in the initial stage of deformation elastically, while plastic deformations set on later in process of a continued loading. [9] And the beginning of plastic deformation is identified by a surface in stress space, so-called the yield surface. The direction of plastic deformations can be obtained with the plastic potential, whereas demands that a stress point carries behind the yield surface, while loading. Therefore, lots of additional notions (mainly of geometric nature) is requested to characterize the elastoplasticity. Aforementioned shortcoming makes that various elastoplasticity constitutive equations are totally hardly tractable, not easy to be performed in FEM-code and highly sensitive to parameters controlling the various involved numerical algorithms. [9]

1.2.3 Hypoplasticity

Aims to determine the above anelastic phenomena without using the additional notions, hypoplasticity is introduced. The ostensible difference between hypoplasticity and elastoplasticity is that anelastic deformations may start the very beginning of the loading process in hypoplasticity. It does not a priori distinguish between elastic and plastic deformation. It means that the distinction between loading and unloading is automatically accomplished by the equation itself.

Before the hypoplasticity, some historical remarks should be mentioned. In his article in 1952, Truesdell drew attention to a concept for constitutive equations by expressing the stress rate as a function of strain rate as follow: (equation 1) where $\ddot{T}$ is the

Jaumann stress rate; L is an isotropic tensorial function of its arguments and is linear in D. This concept was then detailed in a voluminous paper entitled 'Hypoelasticity' in 1955. [11] Packed with numerous graphical representations produced at graphic art division of the US Navy, which was rather unusual for such purely theoretical treatises. In this sense, Truesdell's concept was a pioneer work and the great work in using computer in the research of constitutive equations. [11] And later the physical relevance of hypoelasticity, specially its relation to plasticity theory, was pursued by Thomas (1955) and Green (1956a, 1956b). They found that the behavior upon reversal of strain rate cannot be described with a single hypoelastic equation. Then, Green introduced a rate of stress work as the loading criterion to solve the previous problem with remaining the constitutive equation but adding different coefficients (used for loading and unloading). In the next two decades later, the theory of hypoplasticity experienced a renaissance in modelling the behavior of pressure dependent materials. Here, some progress in applying hypoplasticity to metallic materials notably made by Tokkuoka (1971,1977,1982), was supposed to be the beacon, in particular the ideas of failure. And some theoretical foundation of hypoplasticity was made by Krawietz (1979). And the model included main ingredient of hypoplasticiy was proposed by Kolymbas in 1977. [Kolymbas 1978]

In this research, a formal definition of hypoplasticity provided by Wu and Kolymbas 1990 is used. The hypoplastic constitutive equation shows the stress increasement as a function of a given strain increasement and of the actual stress and void ratio. It defines that the hypoplastic constitutive model by assuming that exists a tensorial function H. Function H consist with two variables, stretching (strain rate) and Jaumann stress rate. (equation 2) Elastoplastic and hypoplastic equations are both of this general

form. There are various hypoplastic constitutive equations developed by different pioneers, e.g. Kolymbas, Gudehus, Bauer, Von Wolffersdorff and Wu. (Kolymbas1995, Gudehus 1996, Bauer1996, Von Wolffersdorff1996, Wu1999b) These models are all on account of the concept above (separate linear and nonlinear part) and will be mentioned in detail later.

1.2.4 Summary

The performed literature review has associated with sketching the historical remarks and means for achieving the goals of this research. Researchers for decades have been exploring hypoplastic constitutive equation to mechanics investigation. In this research, the hypoplastic constitutive equations matched with the true-triaxial test simulation DEM [10] will be explored, further, the parameters work of constitutive model will be discussed. These parameters will be the critical factor in both stress path and yield surface.

1.3 Objectives and Methodology

From extensive literature review, the goal of this research is to first understand how hypoplastic constitutive equation works to account for the granular materials. With the concept introduced by Kolymbas [9], the simple model should be known well. In brief, the concept which the constitutive equation was separated by two parts (linear part and nonlinear part) is easier to be implemented into numerical algorithms and is also easier to be grasped. [9] From this understanding, the yield surface which was already proved to be the significant approach in elastoplastic theory can be investigated with hypoplastic constitutive equation. Simulating a yield surface on pi_plane (pressure-dependent, which will be detailed description in the later section) required to match the results did in the true

triaxial DEM simulation [10]. This challenge has been addressed by making use of a simulation framework for hypoplasticity expatiated later in this thesis.

The present study has the following objectives:

1. Learn the fundamentals of hypoplasticity method.

2. Utilizing hypoplasticity constitutive equation to simulate the normal constitutive model.

3. Establish the framework within the simulation of hypoplasticity constitutive model and match the Lade-Duncan, Mohr-Coulomb, Matsuoka-Nakai yield surface.

4. Get the different parametric results from the fitted hypoplastic constitutive equation.

5. Explore the physical significance of the different parametric in the same hypoplastic framework.

6. Use response envelope method to simulate the several yield criterions as the most hypoplasticity research paper procedure.

7. Research and implement improvements to the optimal hypoplasticity constitutive model.

From aforementioned literature research, this hypoplastic theory has been verified that it can successfully describe the granular media. However, there are several different kinds of hypoplastic constitutive equations in the past almost three decades and it is really tough to make the decision (which one is the best). Every equation has the same concept we already mentioned above but combined lots of personal decisions. Therefore, the

hypoplastic constitutive equation will be investigate based on Kolymbas [9] and combined with the experimental data from a true-triaxial test [10] in this thesis. After matching the DEM simulation result made by Fleischman, the investigation about parametric work will be discussed in the end of this thesis.

2 THEORETICAL BACKGROUND

This chapter provides an overview of theoretical topics relate to this research. To accomplish the objectives of this study, some fundamentals of continuum mechanics should be mentioned. And then the details of hypoplastic constitutive equation are presented. In this chapter, an exhaustive process of formula derivation about hypoplastic constitutive equation will be made. Also, the theoretical knowledge with the yield surface in elastoplasticity which will be digested with the hypoplasticity theory used in this research is the case to be emphasized as well.

2.1 Fundamentals of Continuum Mechanics

Here we simply present the deformation, stretching, Cauchy stress, changing in observer and time rates in continuum mechanics which are just the tip of the iceberg but will be used later in this research.

Let the motion of a granular material point be referred to the fixed rectangular Cartesian coordinates. And the material points with the material (or LAGRANGE) coordinates X_i (i = 1,2,3) move into a position with the spatial (or EULER) coordinates x_j (j = 1,2,3). [9] And the motion and the deformation gradient are defined as equation 2.1 and equation 2.2 separately,

$$x = x(X, t) \quad \text{----------(2-1)}$$

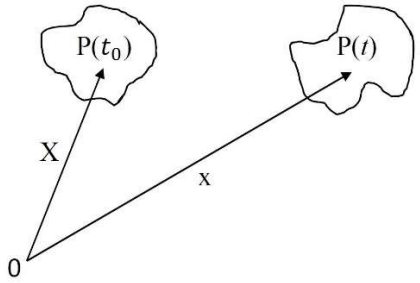

Figure 2-1 x is the position vector at time t for the particle P, and X is the position at time t_0.

$$F = F_{ij} = x_{ij} = \frac{\partial x_i}{\partial X_j} = \frac{\partial x}{\partial X} \text{ ----------(2-2)}$$

where F is the deformation gradient and can be decomposed into

$$F = RU = VR \text{ ----------(2-3)}$$

Here, the rotation R is a properly orthogonal tensor (it means that $R^T = R^{-1}$ and $\det(R) = 1$). U and V are the right and left stretch tensors, separately.

EULER's stretching tensor D,

$$D = D_{ij} = \frac{1}{2}(v_{i,j} + v_{j,i}) = \frac{1}{2}(\dot{x}_{i,j} + \dot{x}_{j,i}) = \dot{x}_{(ij)} \text{ ----------(2-4)}$$

CAUCHY's spin tensor is obtained as the antimetric part of the velocity gradient as follow,

$$W = W_{ij} = \frac{1}{2}(v_{i,j} - v_{j,i}) = \frac{1}{2}(\dot{x}_{i,j} - \dot{x}_{j,i}) = \dot{x}_{[ij]} \text{ ----------(2-5)}$$

And the other two static and kinematic quantities are also used in this paper, the CAUCHY stress tensor and the logarithmic strain tensor. Considering there is a particular point of the cutting surface with the unit normal n and the stress vector t. The relationship above can be account for the equation 2-6, i.e. both vectors are connected by the linear

transformation T, so-called CAUCHY stress tensor. CAUCHY stress tensor can be decomposed in a deviatoric stress tensor (T^*) and a hydrostatic part ($\frac{1}{3}trT1$) as equation 2-7. [9] The logarithmic tensor is defined as equation 2.8, where V is the left stretch tensor as aforementioned and follows from the polar decomposition of the deformation gradient. As a useful strain measure in one dimension and also in two and three dimensions when the principal axes of strain are fixed, the logarithmic tensor can be considered as the time rate of the strain measure in this thesis (special case i.e. W=0, D is the time rate of logarithmic strain ε_{ij}). [12]

$$t = Tn \quad \text{----------(2-6)}$$

$$T = T^* + \frac{1}{3}(trT)1 \quad \text{----------(2-7)}$$

$$E = \ln V \quad \text{----------(2-8)}$$

At this point, a material behavior should be mentioned. If the stress is transformed according to $T^* = QTQ^T$, where Q is regarded as the rotation, this material behavior can be called *independent of the observer* (all tenors transformed according this relationship are so-called *independent of the observer*). Here, introducing the JAUMANN stress rate as follow:

$$\ddot{T} = \dot{T} + TW - WT \quad \text{----------(2-9)}$$

where $\ddot{T}$ is the co-rotational or ZAREMBA (often attributed to JAUMANN) stress rate and W denotes the spin tensor. $\ddot{T}$ is the stress change that arise exclusively from the deformation of the considered material, whereas any other apparent parts are removed, because of rotations of the observer or of the reference frame. And the *principle of material*

frame-indifference, so-called *objectivity*, requires that the stress T in a constitutive equation should be determined through the equivalent motion above, i.e. $T^* = QTQ^T$. In brief, derivation of vectorial and tensorial quantities with respect to time imposes problems if they refer to a material (or so-called 'concomitant') vector basis: the only change of the reference frame gives rise to a non-vanishing time derivative of the considered quantity. (p.26 in [9]) Therefore, we introduce several methods to describe the objective time rates, i.e. time rates that are free of apparent terms [13]. In this paper, we select JAUMANN stress rate as the fundamental method to describe the objective time rates which will be expended in later sections.

JAUMANN	$\ddot{T} := \dot{T} + \mathrm{TW} - \mathrm{WT}$
OLDROYD	$\mathcal{L}\mathrm{T} := \dot{T} - \mathrm{T}L^T - \mathrm{LT}$
Convected stress rate	$T^{\Delta} := \dot{T} + \mathrm{TL} + L^T\mathrm{T}$
GREEN-MCINNIS-NAGHDI	$T^{\blacksquare} := \dot{T} + \mathrm{T}\Omega - \Omega\mathrm{T}$

2.2 Hypoplasticity Background

2.2.1 Rate Equation

A constitutive equation is aim at illustrating stress due to a strain (or deformation) history starting from some specific reference state. (p33 in [9]) In order to represent history (or path) dependence in physics the general method is introduced, which is to use non-integrable differential forms (PFAFFEAN forms). It is equation 2-10, representing y by the differential equation and connecting increments dx_1, dx_2,…with dy.

$$dy = a_1 dx_1 + a_2 dx_2 + \ldots a_n dx_n \text{ ----------(2-10)}$$

It can also be rewritten as $dy = f(dx_i)$ (it is not integrable), as the general way to procced soil mechanics. When it represents the stress increment as a non-integrable function of the strain increment, here stress "σ" and strain "ε" are substituted into the equation above, then, as equation 2-11:

$$d\sigma = f(d\varepsilon) \text{ ----------(2-11)}$$

$$\dot{\sigma} = \frac{d\sigma}{dt} \text{ ----------(2-12)}$$

$$\dot{\varepsilon} = \frac{d\varepsilon}{dt} \text{ ----------(2-13)}$$

With dividing all increment by *d*t, equation 2-12 and 2-13 show the time rates. Then, substituting "$\dot{\sigma}$" and "$\dot{\varepsilon}$" into equation 2-11, $\dot{\sigma} = f(\dot{\varepsilon})$ is obtained, so-called rate equation. Thus, with the tensor notation, previous rate equation will be obtained as $\ddot{T} = f(D)$, where $\ddot{T}$ denotes the JAUMANN stress rate which is defined as equation 2-9.

As aforementioned, a formal definition of hypoplasticity has been provided by Wu and Kolymbas [1990]. Defining that the hypoplastic constitutive model is assumed by the tensorial function H (equation 2-14),

$$\ddot{T} = H(T, D) \text{ ----------(2-14)}$$

where T denotes the Cauchy stress tensor and D denotes the stretching (strain rate). And we assume that the function H (2-14) is continuously differentiable for all D except at D = 0.

Herein, the point should be noted that function H is a rate-equation. Generally, we define the stress as the function of strain, but it also means that the stress does not depend on the deformation history which is so-called elastic behavior. [9] Due to soil's behavior (aforementioned in chapter 1), plastic property can't be disregarded in the constitutive equation for soil. The general method to introduce history dependence in physics is to utilize the non-integrable differential forms. [9]

Therefore, the constitutive equation is introduced in this version (equation 2-15), where $\dot{T} = \ddot{\mathrm{T}}$, note that, should be the special case in this paper (refer to equation 2-9, W = 0), and D denotes the time rate of logarithmic strain as aforementioned. And equation 2-15 can be expanded as equation 2-17, where φ_i are scalar function of invariants and joint invariants of T and D. (p.38 in [9])

$$\dot{T} = h(T, D) \text{ ----------(2-15)}$$

2.2.2 Restriction on the Constitutive Equation

Here, it should be emphasized that T and D should be homogeneous (in order to describe proportional stress paths in case of proportional strain paths and describe the rate-independent material respectively), here, λ is a scalar quantity which is greater than zero.

$$h(\lambda T, D) = \lambda^n h(T, D) \text{ ----------(2-16)}$$

Since the equation 2-15 is too abstract to represent a specific constitutive model, some restrictions are necessary to be imposed on the function h in equation 2-15. Equation 2-17 is introduced as the general representation theorem. [9]

$$\mathrm{h(T,D)} = \varphi_1 1 + \varphi_2 T + \varphi_3 D + \varphi_4 T^2 + \varphi_5 D^2 + \varphi_6(TD + DT) + \varphi_7(TD^2 + D^2T) + \varphi_8(T^2D + DT^2) + \varphi_9(T^2D^2 + D^2T^2)$$ ----------(2-17)

where φ_i are scalar functions of invariants and joint invariants of T and D.

Otherwise, hypoplasticity linear in both T and D. Equation 2-18 is one case of various hypoplasticity constitutive equation from [11]

$$\ddot{T} = \dot{T} = C_1(TD + DT) + C_2\frac{tr(TD)}{trT}T + C_3\frac{T^3}{trT^2}\sqrt{trD^2} + C_4\frac{(T^*)^2}{trT}\sqrt{trD^2}$$ ----------(2-18)

2.3 Yield Surface

From previous literature review, the yield surface was known as a significant method to predict macro-scale failure. And Drucker-Prager, Mohr-Coulomb, Matsuoka-Nakai and Lade-Duncan yield surfaces played the great roles in the investigating mechanism of granular materials. And it was verified that Lade-Duncan yield surface has the best performance in all four yield surfaces aforementioned by empirically experiment. Figure 2-2(b) shows the intersection of all four yield surfaces with the plane (also called π-plane) of constant hydrostatic pressure p. All four yield surfaces projected on the π-plane are calibrated to match in pure compression as illustrated in Figure 2-2(a) and (b).

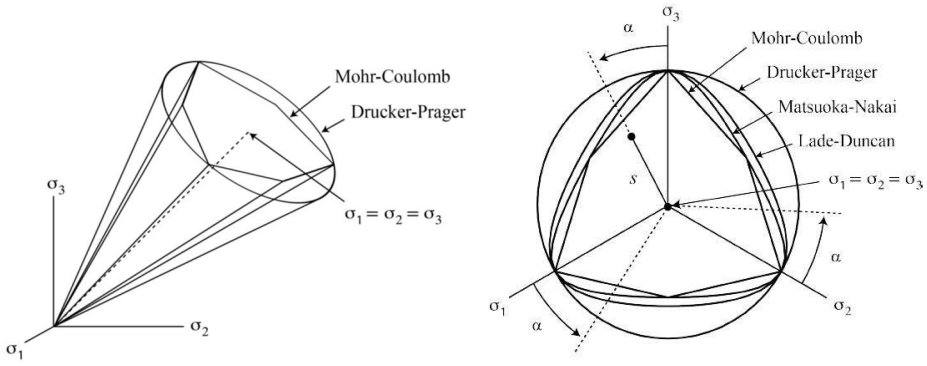

Figure 2-2 (a)(b) (a). Yield surface viewed as cones in principal stress space and (b). intersection of Mohr-Coulomb, Drucker-Prager, Matsuoka-Nakai and Lade-Duncan yield surfaces with the π-plane.

Mohr-Coulomb yield criterion is the oldest yield criteria for particulate materials in general, and for geomaterials in particular. [10] And it can be characterized in terms of three main items (p, s and α), which are hydrostatic pressure, the scalar magnitude of the deviatoric stress and the lode angle respectively. As a simple cycle projected on the π-plane, Drucker-Prager yield surface is the most imprecise one, which is the pressure dependence only (compared with Mohr-Coulomb yield criterion, it is no lode angle dependence), as showed in Figure 2-2(a) and (b).

For non-cohesive materials (or granular materials), the Matsuoka-Nakai yield surface [14] is characterized in principal stress space by surface $I_1 I_2 / I_3 = C_{MN}$, where the I_1, I_2 and I_3 are the principal stress invariants (invariants are given in terms of the principal stresses by $I_1 = \sigma_1 + \sigma_2 + \sigma_3$, $I_2 = \sigma_1\sigma_2 + \sigma_2\sigma_3 + \sigma_3\sigma_1$ and $I_3 = \sigma_1\sigma_2\sigma_3$). Lade-Duncan yield surface [15] is defined with C_{LD}, which is given by ${I_1}^3 / I_3 = C_{LD}$. Compared with the material strength parameter of Matsuoka-Nakai yield criterion, Lade-Duncan's parameter has the same denominator, and the similar combination of numerator (as $I_i I_j$). Then, the parameter which generalized the Drucker-Prager yield surface is characterized in principal stress space by surface ${I_1}^2 / I_2 = C_{DP}$. [10]

3 EXPERIMENTAL SET UP

This chapter introduce the hypoplastic constitutive model for granular materials. Based on the original hypoplastic constitutive equation (proposed by D. Kolymbas aforementioned in previous chapter), the improved model is developed to match four yield criterions (Drucker-Prager, Mohr-Coulomb, Matsuoka-Nakai and Lade-Duncan) which were generated by elasto-plastic method.

3.1 Yield Surface in Elasto-plasticity

3.1.1 Material Strength Parameters

As simply aforementioned in chapter 1.2.3, the elasto-plastic method has been a good way to predict the behavior of granular material with the similar constitutive model (i.e. decomposition of strain into elastic and plastic parts, but in hypoplastic decomposition of stress rate into linear and non-linear parts) before hypoplastic theory was proposed. It is not necessary to say which method is the best, but to take the advantage from each method.

Through the numerical elasto-plastic continuum-based methods, all four yield surfaces are projected on the SMP i.e. spatially mobilized plane [14]. The Mohr-Coulomb failure state is defined by the "Coulomb friction" criterion which can be simply characterized by equation3.1,

$$\max\left(\frac{|\sigma_i-\sigma_j|}{2\sqrt{\sigma_i\sigma_j}}\right) = \mu_{macro}, i,j = 1,2,3 \text{ ----------(3-1)}$$

$$\mu_{macro} = \left(\frac{\sigma_t}{\sigma_n}\right)_{max} \text{----------(3-2)}$$

Where μ is the coefficient of (Coulomb) friction corresponding to the ratio of tangential to normal stress on any plane. And this marcro-scale coefficient μ is obtained by $\mu = \tan\Phi$, where Φ is the material friction angle. In contrast to the Mohr-Coulomb yield surface, the Drucker-Prager yield criterion which is pressure dependence only can be characterized in principal stress space by the surface $s/p = k$, where s is the scalar magnitude of the deviatoric stress tensor, p is the hydrostatic pressure, and k is a material strength parameter. And in this paper, k can be obtained in term of equation 3-3.

$$k = \sqrt{\frac{2}{3}} * \frac{6\sin\Phi}{3-\sin} \text{ ----------(3-3)}$$

And as already mentioned in previous chapters, Matsuoka-Nakai yield criterion and Lade-Duncan yield criterion are characterized in principle stress space by the surface $I_1 I_2 / I_3 = C_{MN}$ and by the surface ${I_1}^3 / I_3 = C_{LD}$, respectively, where I_1, I_2 and I_3 are the principal (scalar) stress invariants. For the objective of comparison, parameter of Drucker-Prager yield criterion can be rewritten as ${I_1}^2 / I_2 = C_{DP}$, where C_{DP} is a material strength parameter specific to this form of the model. [10] Table 3-1 shows all four parameters which will be used to characterize the yield surface. Here, these four parameters should not be confused with the hypoplastic parameter $C_i, i = 1,2,3,4$, even though the notation of these parameter are all with capital 'C'.

Table 3-1. Material strength parameters for Mohr-Coulomb, Drucker-Prager, Matsuoka-Nakai, and Lade-Duncan criteria.

C_{MC}	C_{DP}	C_{MN}	C_{LD}

μ	$\frac{{I_1}^2}{I_2}$	$\frac{I_1 I_2}{I_3}$	$\frac{{I_1}^3}{I_3}$

3.1.2 Calibration

With all four material strength parameters, four yield surfaces can be generated. Nevertheless, these four criterions are not useful without calibration i.e. adapting together with several fixed points or specific points on the projected Spatially Mobilized Plane. Two specific positions which are pure compression and pure extension should be emphasized. And some shape factors are necessary to be introduced here, i.e. α, b and λ, where λ can be characterized through equation 3-4, α is the Lode Angle and b can be obtained by the equation in term of λ (equation 3-5).

$$\lambda = \frac{s_2}{s_3} \text{ ----------(3-4)}$$

$$\mathrm{b} = \frac{1+2\lambda}{2+\lambda} \text{ ----------(3-5)}$$

where s is the deviatoric stresses and these stresses are ordered from smallest to largest such as $s_1 \leq s_2 \leq s_3$; $\alpha = \tan^{-1}[(1+2\lambda)/\sqrt{3}]$ by $-1/2 \leq \lambda \leq 1$ and $0 \leq \alpha \leq 60^o$, as defined in [16] and the intermediate stress ratio $\mathrm{b} = (s_2 - s_1)/(s_3 - s_1) = (\sigma_2 - \sigma_1)/(\sigma_3 - \sigma_1)$ where $0 \leq \mathrm{b} \leq 1$ characterized by equation 3.5, (where σ_1, σ_2 and σ_3 must all be positive in a structurally-stable non-cohesive particulate or granular material), as defined in [17].

It exists two significant limit positions or loading states, one is the pure or simple compression which is corresponded with the minimal values of three parameters i.e. $\lambda = -1/2$, $\alpha = 0$ and $\mathrm{b} = 0$, the other is the pure or simple extension with the maximal values

of three metrics, $\lambda = 1$, $\alpha = 60^o$ and $b = 1$. Also, limit positions result the corresponding deviatoric stresses, as $s_1 = s_2 = -s_3/2$ where $s_1 = s_2 < 0 < s_3$ during the pure compression. And under the pure extension condition, $s_1 < 0 < s_2 = s_3$ and $s_2 = s_3 = -s_1/2$.

Table 3-2. Specific Lode Angle correspond with the limit condition.

α	0	16^o	30^o	44^o	60^o
Condition Description	Pure Compression				Pure Extension

Here, all four yield criterions should be matched at the point i.e. pure compression in other words: $\alpha = 0$. And all yield surfaces must be independent of the sign ($\pm$) of the Lode angle α, and posses 120^o rotation symmetry on the π-plane as already showed in Figure 2-2b.

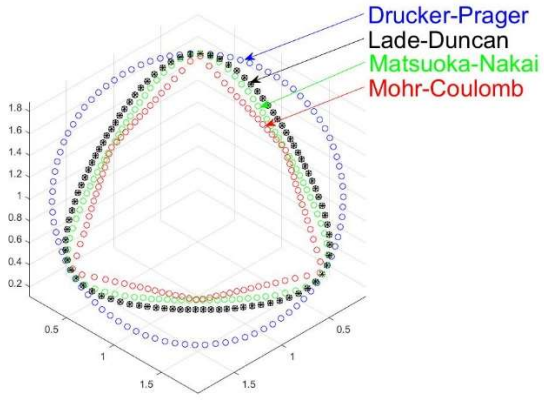

Figure 3-1. Calibrated four yield surfaces through Elasto-plastic Method

Therefore, in order to explore how the Hypoplasticity can work with the yield criterion, all these four yield criterions which calibrated as figure 3-1 should be generated to the yield surfaces through the hypoplastic method.

3.2 Hypoplastic Model Description

The hypoplastic constitutive model is developed based on the original concept model equation 2-10 which is generated to the more detailed version equation 2-14 aforementioned in 2.2.2. And it is capable of capturing some salient features of granular materials, e.g. nonlinearity, failure and dilatancy. As already detailed description in section 2.2.2, in analogy to two main variables in this paper stress (σ) and strain (ε), it can be assumed that the constitutive equation 2-14 can be decomposed into these two variables and representing the linear and non-linear part as equation 3-6,

$$\ddot{\sigma} = L(\sigma, \dot{\varepsilon}) + N(\sigma, \dot{\varepsilon}) \text{ ----------(3-6)}$$

Where term of L is linear in $\dot{\varepsilon}$ and term of N is non-linear in $\dot{\varepsilon}$. Concrete expressions for $L(\sigma, \dot{\varepsilon})$ and $N(\sigma)$ can be obtained by invoking the representation theorem for isotropic tensorial functions. [11] Therefore, the tensor notation T and D is substituted in equation 3-6 as

$$\ddot{T} = LD + N|D| \text{ ----------(3-7)}$$

Here, in terms of linear part, "L" is regarded as the linear operator applied to "D". And it is to summarize non-linear terms by $N|D|$ with $|D| = \sqrt{trD^2}$. Then, in order to not be confused with the notation of stress or strain, here, some aforementioned notations will

be recalled. $\ddot{T}$ denotes the JAUMANN stress rate which is defined as equation 2-9, T denotes the Cauchy stress tensor, D denotes the stretching (strain rate). [9]

Another important factor is that, strictly speaking, D is not the time rate of any strain measure and it is the time rate of logarithmic strain tensor. There is the particular process of proof in Anne Hoger's dissertation 1986. The result of proof i.e. $\ln(\mathrm{V})^* = \mathrm{D}$ (where V is the left stretch tensors and D) is used directly in this paper (in other words, the corotational and JAUMANN derivatives of $\ln(\mathrm{V})$, and establish conditions under which these logarithmic strain rates are equal to the stretching tensor). [12]

Thus, the linear operator should be the fourth order tensor and $\ddot{T}$, D and N are second order tensors. It seems much more obvious with the tensorial notation i.e. $\ddot{T}_{ij} = L_{ijkl}D_{kl} + N_{ij}|D|$. Then, the constitutive equation can be recast in the form by virtue of Euler's theorem for homogeneous functions,

$$\ddot{T} = HD \text{ ----------(3-8)}$$

where

$$\mathrm{H} := \mathrm{L} + \mathrm{N} \otimes D^0 \text{---------(3-9)}$$

In which D^0 is the normalized stretching and $D^0 := \frac{D}{|D|}$ and the symbol "$\otimes$" denotes an outer product in matrix multiplication (or tensor multiplication). It is worth noting that the forth order tensor L is, in analogy to the elastic stiffness matrix. And the forth order tensor H represents the tangential stiffness matrix. It shows that tangential stiffness is not only stress dependence but also standing for the direction of strain rate. And there is not necessary to distinguish between loading and unloading in hypoplasticity due to the non-linear part is always active for both loading and unloading. [11]

3.3 Hypoplastic Constitutive Model

3.3.1 General Model

Then, in this section, a similar constitutive equation (equation 3-10) with the same components is introduced, which was obtained in Wu's dissertation 1992. The reason for preferring the equation 3-10 is that it is quite simple (comparing with equation 2-14) and it is as satisfactory as equation 2-14. (And some further exploration with equation 2-14 will be mentioned in later chapter 4) Thus, T^* denotes the deviatoric stress (equation 3-10) and C_i where $i = 1,2,3,4$ are the material constants (will be discussed in chapter 4) in equation 3-7.

$$\ddot{T} = C_1(trT)D + C_2\frac{tr(TD)}{trT}T + C_3\frac{T^2}{trT}\sqrt{trD^2} + C_4\frac{(T^*)^2}{trT}\sqrt{trD^2} \text{ ----------(3-10)}$$

$$T^* = T - \frac{1}{3}(trT)1 \text{ ----------(3-11)}$$

Due to the stress rate $\dot{T}$ which already mentioned in previous chapter 2.2.1, the stress path can be obtained through equation 3-12. It should be noted that the JAUMANN stress $\ddot{T}$ is equivalent to the stress rate $\dot{T}$ under circumstances (due to rotations of observer or of the reference frame, the rotation tensor W parts are removed).

$$T_{i+1} = T_i + \dot{T}_i * t,\ i = [0, \infty] \text{ ----------(3-12)}$$

3.3.2 Limit States of Hypoplasticity

There is a quote from W. WU and D. KOLYMBAS, "we have to bother about the definition for a phenomenon that is nearly as soil mechanics itself, since failure is defined

in the context of the constitutive equation in concern". As one of the most important property of the granular materials, the ability to yield (or flow) should be emphasized here.

The ability to yield, it is to undergo large deformations without stress change, as soon as the stresses and the void ratio obtain their critical values. And this sort of flow should be regarded as 'plastic' flow and distinguished from the flow of fluids. [9]

When a material element is said to be at the limit state (or failure), for the given stress σ, there exists a strain rate $\dot{\varepsilon}$ fulfil the equation as follow,

$$\ddot{\sigma} = H(\sigma, \dot{\varepsilon}) = 0 \text{ ---------- (3-13)}$$

With the tensorial notation, equation can be recast as,

$$\ddot{T} = \mathrm{h(T, D)} = 0 \text{ ----------(3-14)}$$

Here, equation 3-13 is the yield function which is also contained in a hypoplastic formulation $\ddot{T} = \mathrm{h(T, D)}$, i.e. the yield function f(T) can be obtained from the constitutive relationship. Therefore, combined with yield function, the equation 3-7 can be rewritten as

$$\ddot{T} = \mathrm{L(T)}[D] + N(T)|D| = L(T)[D + B|D|] \text{ ----------(3-15)}$$

Where $D^0 := \frac{D}{|D|}$ is defined as $\frac{D}{|D|} = -\mathrm{B}$. Here, if $\ddot{T} = 0$, it occurs $D + B|D| = 0$, where L(T) is a matrix operator applied to its tensorial argument (two factors part in equation 3-15).

Consequently, the function f(T) reads

$$\mathrm{f(T)} = \mathrm{tr}B^2 - 1 = 0 \text{ ----------(3-16)}$$

As the definition of B, the constitutive equation 3-10 can be recast as

$$\mathrm{B} = L^{-1}N = \frac{C_3 T^2}{C_1(trT)^2} + \frac{C_4 T^{*2}}{C_1(trT)^2} - \left(\frac{C_2 C_3}{C_1}\frac{tr(T^3)}{(trT)^2} + \frac{C_2 C_4}{C_1}\frac{tr(TT^{*2})}{(trT)^2}\right) \times \frac{T}{C_1(trT)^2 + C_2 tr(T^2)} \text{-------(3-17)}$$

Because of homogeneity of B in T, the surface $\mathrm{f(T)} = \mathrm{tr}B^2 - 1 = 0$ is a cone with apex at the origin $\mathrm{T} = 0$ [9], which is in analogy to elastoplastic yield surface [10].

3.3.3 Specific Model

From previous chapter, the hypoplastic model and the limit states are introduced. And the parameters $C_i, i = 1,2,3,4$, are the specific material constants. In this chapter, some specific material coefficients are introduced to validate the effect of the hypoplastic constitutive model.

Table 3-3. Parameters of material constants for specific granular material. [9]

C_1	C_2	C_3	C_4
-106.5	-801.5	-797.1	1077.7

With the material coefficient (showed in Table 3-3) for one specific granular material provided by D, Kolymbas 1999, most of general material mechanism (i.e. stress history.) is determined through aforementioned hypoplastic constitutive model, e.g. with the initial condition such as initial stress state equation 3-18 and constant D equation 3-19, stress path can be determined (showed in figure 3-2).

$$\mathrm{T} = \begin{pmatrix} 150 & 0 & 0 \\ 0 & 100 & 0 \\ 0 & 0 & 100 \end{pmatrix} (kN/m^2) \text{----------(3-18)}$$

$$D = \begin{pmatrix} -\cos\alpha & 0 & 0 \\ 0 & -\sin\alpha/\sqrt{2} & 0 \\ 0 & 0 & -\sin\alpha/\sqrt{2} \end{pmatrix} \text{----------(3-19)}$$

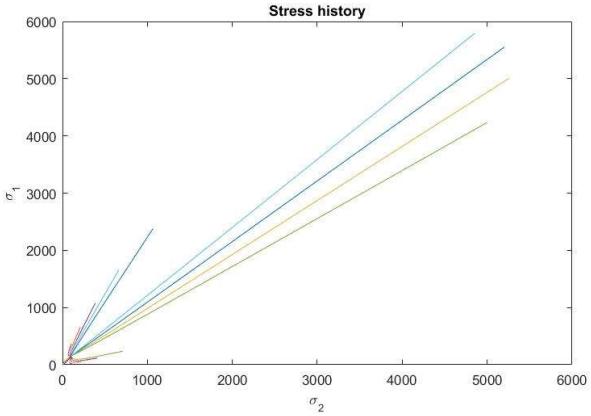

Figure 3-2. Stress History by Hypoplasticity Model with initial condition Equation 3-18 & 3-19

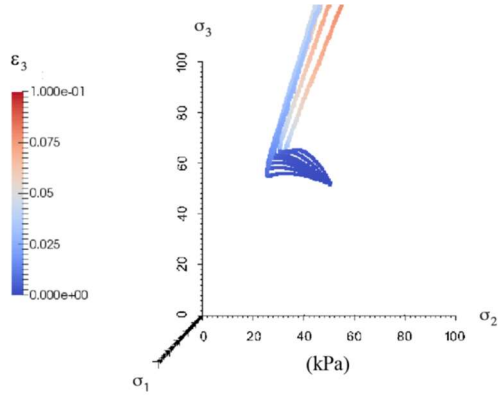

Figure 3-3. Partial yield cone formed by the stress paths corresponding to the true-triaxial test for the DEM simulation in [10]

Comparing the stress path determined from hypoplastic constitutive model with the stress path obtained from the DEM true-triaxial test simulation, it is obviously that hypoplasticity model has the capacity to fully describe the granular materials. As the geometric definition of the yield surface which is that the yield surface can be viewed as the intersecting surface of the stress path in 3-D rectangular coordinate system (or the cone in the Figure 2-2a) with the π-plane at the specific hydrostatic pressure, the success of

matching the stress path as a cone is all-important. Note that, the purpose of this section which aforementioned in previous chapter, is to match the yield criterion with hypoplastic model and DEM simulation. Therefore, due to the validation of the hypoplasticity, the further work with the failure surface can be proceeded.

3.3.4 Improved Yield Surface with Hypoplasticity

The existing yield surface characterized with elasto-plastic method projects three principal stress directions onto the π-plane, which corresponding with three shape factors i.e. λ, α and b aforementioned in the chapter 3.1. Due to the validation that the hypoplastic stress path was generated in the previous section, it should exist a closed "cycle" or a "triangle" with radians on the π-plane corresponding with the hydrostatic pressure *p*.

According to the limit states of hypoplasticity, the constitutive equation B which is the second order tensor can be rewritten as follow,

$$B = \begin{pmatrix} B(1) & 0 & 0 \\ 0 & B(2) & 0 \\ 0 & 0 & B(3) \end{pmatrix} \text{--------(3-20)}$$

Substituting $I_1 = \sigma_1 + \sigma_2 + \sigma_3 = tr(T)$ into equation 3.17, where $\sigma_i, i = 1,2,3$ are the components of the second order tensor T (also can be denoted by T(i)).

$$\mathrm{B}(1) = \frac{C_3(T(1))^2}{C_1(I_1)^2} + \frac{C_4 T^{*2}}{C_1(I_1)^2} - \left(\frac{C_2C_3}{C_1}\frac{tr(T^3)}{(I_1)^2} + \frac{C_2C_4}{C_1}\frac{tr(TT^{*2})}{(I_1)^2}\right) \times \frac{T(1)}{C_1(I_1)^2 + C_2 tr(T^2)} \text{--------(3-21)}$$

$$\mathrm{B}(2) = \frac{C_3(T(2))^2}{C_1(I_1)^2} + \frac{C_4 T^{*2}}{C_1(I_1)^2} - \left(\frac{C_2C_3}{C_1}\frac{tr(T^3)}{(I_1)^2} + \frac{C_2C_4}{C_1}\frac{tr(TT^{*2})}{(I_1)^2}\right) \times \frac{T(2)}{C_1(I_1)^2 + C_2 tr(T^2)} \text{--------(3-22)}$$

$$\mathrm{B}(3) = \frac{C_3(T(3))^2}{C_1(I_1)^2} + \frac{C_4 T^{*2}}{C_1(I_1)^2} - \left(\frac{C_2C_3}{C_1}\frac{tr(T^3)}{(I_1)^2} + \frac{C_2C_4}{C_1}\frac{tr(TT^{*2})}{(I_1)^2}\right) \times \frac{T(3)}{C_1(I_1)^2 + C_2 tr(T^2)} \text{--------(3-23)}$$

where $T^* = \mathrm{T} - (I_1/3)\mathrm{I}$ or $T^*(i) = T(i) - I_1/3, i = 1,2,3$. In addition, because of second order tensor B and T are both diagonal tensors, $\mathrm{tr}(T^3)$, $tr(TT^{*2})$ and $tr(T^2)$ can be defined as follow,

$$\mathrm{tr}(T^3) = [T(1)]^3 + [T(2)]^3 + [T(3)]^3 \text{ --------(3-24)}$$

$$tr(TT^{*2}) = \mathrm{T}(1) * [T(1) - I_1/3]^2 + T(2) * [T(2) - I_1/3]^2 + T(3) * [T(3) - I_1/3]^2 \text{ ---(3-25)}$$

$$tr(T^2) = [T(1)]^2 + [T(2)]^2 + [T(3)]^2 \text{ --------(3-26)}$$

Then, substitute all the equations above into equation 3-27 which is known as the yield function in hypoplasticity.

$$\mathrm{tr}(B^2) = 0 \text{ --------(3-27)}$$

$$[B(1)]^2 + [B(2)]^2 + [B(3)]^2 = 0 \text{ --------(3-28)}$$

Note that, parameters $C_i, i = 1,2,3,4$ are references to Table 3-3 first. With solving the function 3-28, the hypoplastic yield surface is generated as figure 3-4.

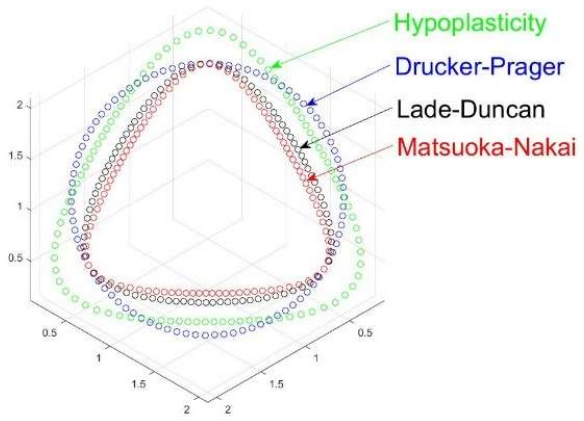

Figure 3-4. Hypoplasticity yield surface in terms of $C_i, i = 1,2,3,4$ in Table 3-3, matching with Drucker-Prager, Matsuoka-Nakai and Lade-Duncan yield surface in elasto-plasticity.

It is obvious that the shape of hypoplastic yield surface is similar with the shape of both Matsuoka-Nakai and Lade-Duncan yield surfaces, not like Drucker-Prager version which the cross-section of the yield surface with the π-plane is a cycle. Without calibrating at the so-called pure compression point, this hypoplastic yield surface over-predicts the strength of the granular material for any loading state. But under-prediction is pronounced for Lode angle $\alpha = 60^o$ or pure extension comparing with Lade-Duncan yield surface.

Due to the definition of hypoplastic theory, the shape of yield surface can be calibrated by adjusting the parameters C_i. Nevertheless, there is not have a clue that 'how to get these parameters?'. From the [18], it says that C_i are the dimensionless constants which can be calibrated with triaxial compression tests. But in this chapter, it is totally empirical way to obtain C_i. According to the permutation and combination, there are 16 combinations of C_i, where i equal 4, as Table 3-4.

Table 3-4 Sixteen probabilities of C_i, where i equal 4, are used to calibrate pure compression.

Probability	C_1	C_2	C_3	C_4
Case 1	Increase	Increase	Increase	Increase
Case 2	Increase	Increase	Increase	Decrease
Case 3	Increase	Increase	Decrease	Increase
Case 4	Increase	Increase	Decrease	Decrease
Case 5	Increase	Decrease	Increase	Increase
Case 6	Increase	Decrease	Increase	Decrease

Case 7	Increase	Decrease	Decrease	Increase
Case 8	Increase	Decrease	Decrease	Decrease
Case 9	Decrease	Increase	Increase	Increase
Case 10	Decrease	Increase	Increase	Decrease
Case 11	Decrease	Increase	Decrease	Increase
Case 12	Decrease	Increase	Decrease	Decrease
Case 13	Decrease	Decrease	Increase	Increase
Case 14	Decrease	Decrease	Increase	Decrease
Case 15	Decrease	Decrease	Decrease	Increase
Case 16	Decrease	Decrease	Decrease	Decrease

Here, the improvement is starting from the case showed in table 3-3, where the case is needed to be calibrated. Setting up the variable Δ, then the table 3-4 can be fulfilled with sixteen different cases e.g. $C_i = {C_i}^0 \pm \Delta$, where ${C_i}^0$ refers the parameter in table 3-3. The result as Figure 3-5 is the result of the cases aforementioned.

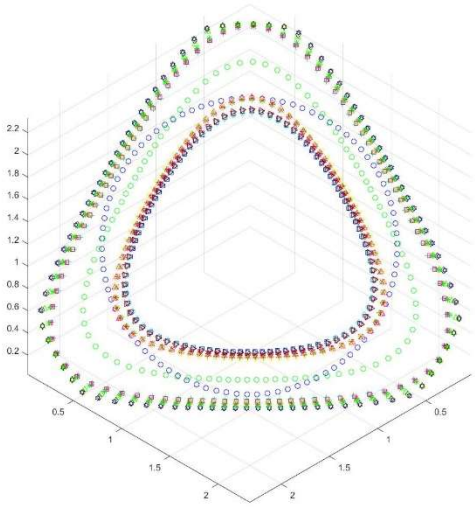

Figure 3-5. Sixteen cases (Δ=20) calibrated with Hypoplastic model in [9], Drucker-Prager, Matsuoka-Nakai and Lade-Duncan yield surface in elasto-plasticity

And each case is detailed in Figure 3-6, as follow,

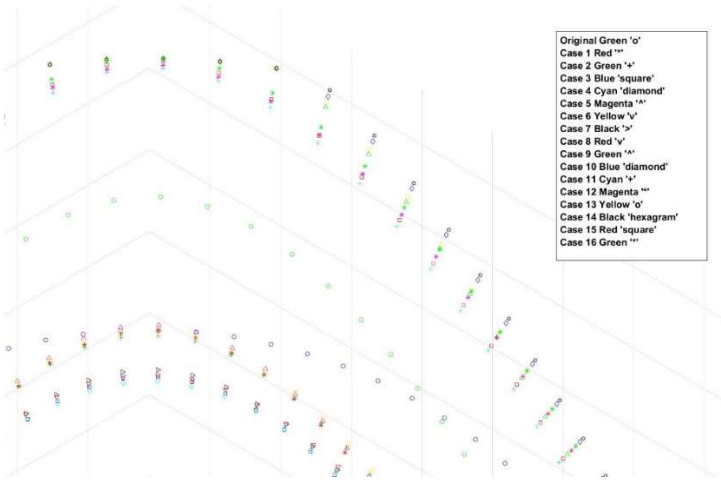

Figure 3-6. illustration of sixteen cases on the π-plane

It is easy to figure out that the yield closed shape expands in cases 9-16 where C_1 is decreased in each case i.e. 9-16. Then, considering the cases 1-8, it is clearly that cases 1,2,5and 6 did great jobs, relatively speaking. Note that, the results above have the precondition i.e. Δ=20 which is hard to convince that parameter C_i should be changed through case 1,2,3 and 6. Therefore, the calibration is also operated with Δ=1, 10, 15 and 25.

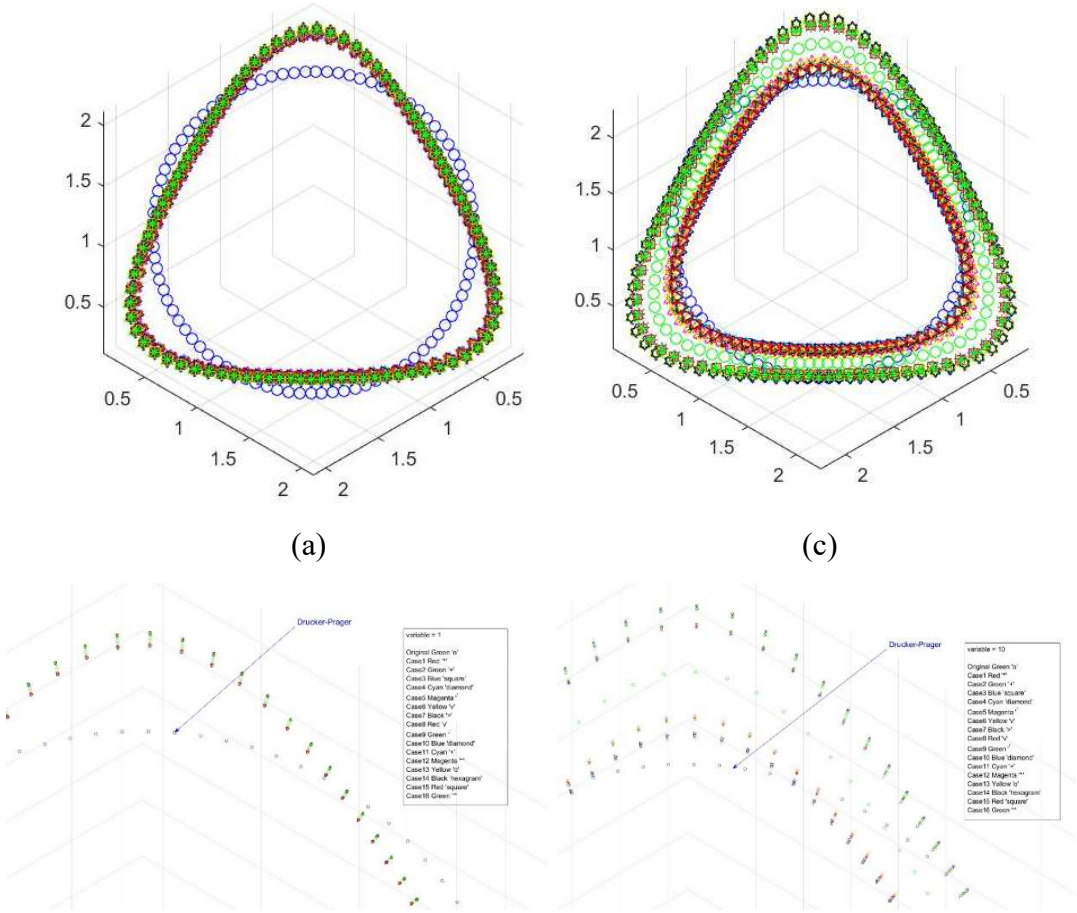

Figure 3-7(a)(b)(c)(d) illustration of sixteen cases on the π-plane with (a)(b) Δ=1 and (c)(d) Δ=10.

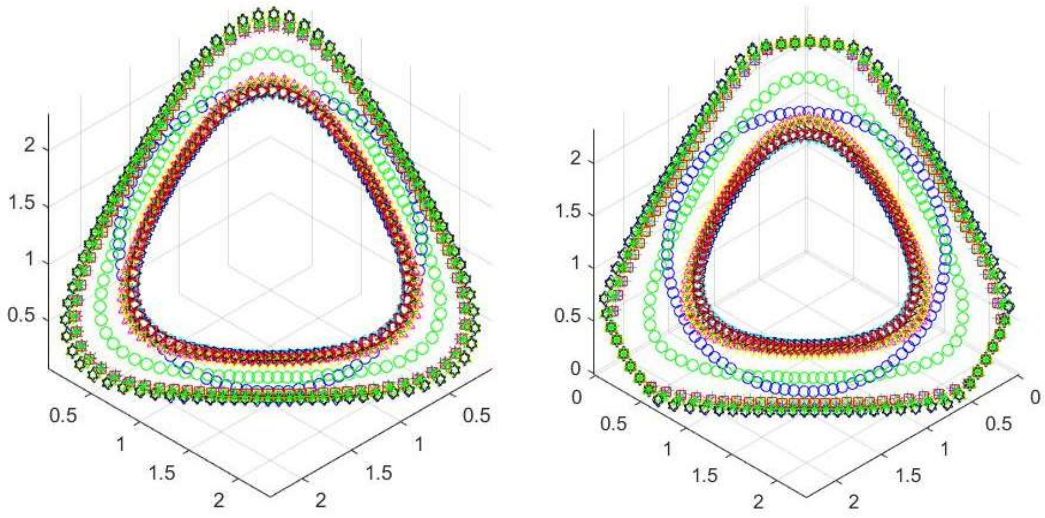

(e) (g)

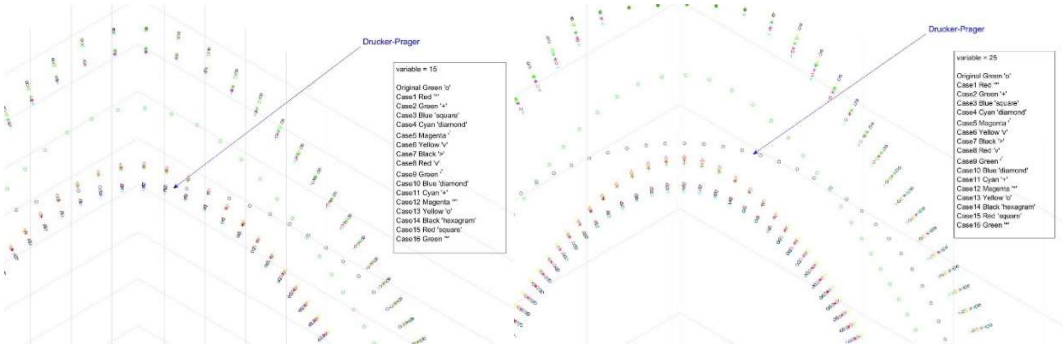

(f) (h)

Figure 3-7(e)(f)(g)(h) illustration of sixteen cases on the π-plane with (a)(b) Δ=15 and (c)(d) Δ=25.

Then, it is not hard to find that all the cases shifted inconspicuously on both sides at the beginning, where Δ=1, in figure 3-7(a)&(b). And cases 1-8 start to approach the calibrated point (pure compression) showed in figure 3-7(c)&(d), which illustrated as small blue ring i.e. marked as Drucker-Prager yield criterion, where Δ=10. In this initial condition, the shapes of all the cases yield surfaces are still overpredicted at the pure compression point or Lode angle α = 0, but it keeps the shapes that seem like Lade-Duncan and Matsuoka-Nakai yield surfaces. Increasing with the number of Δ i.e. variable equal 15, it shows that cases 3,4,7 and 8 start to match the Drucker-Prager yield surface at the peak point on the π-plane. Comparing with the results in figure 3-6, cases 3,4,7 and 8 shrank too much when Δ=20, and cases 1,2,3 and 6 do not start to approach peak point before that the value of Δ is as big as 20. Moreover, it is less-predicted when the number of Δ is too large, such as 25, showed in figure 3-7(g)&(h).

It is interesting that not only considering about the addition and subtraction relation but also the exponential relation will impact the shape of the yield surface. Table 3-4 can

be substituted in terms of $C_i = {C_i}^0 * \Delta$ *or* $C_i = {C_i}^0/\Delta$, where ${C_i}^0$ refers the parameter in table 3-3. Then, the results are generated and shown in figure 3-8(a)(b)(c)(d)(e)(f) where $\Delta = 10$ in figure 3-8(a)(b), $\Delta = 100$ in figure 3-8(c)(d) and $\Delta = 1000$ in figure 3-8(e)(f). Drucker-Prager yield criterion is still displayed as the reference substance in each condition. And it is tracked that the shapes of yield surface are shrunk very small and are transforming much smaller with the increasing of the variable Δ in cases 5,6,9,10,11,13,14 and 15 (it is obvious in figure 3-8(a)(c)(e), red close figure trail off as a small cycle in figure (e)).

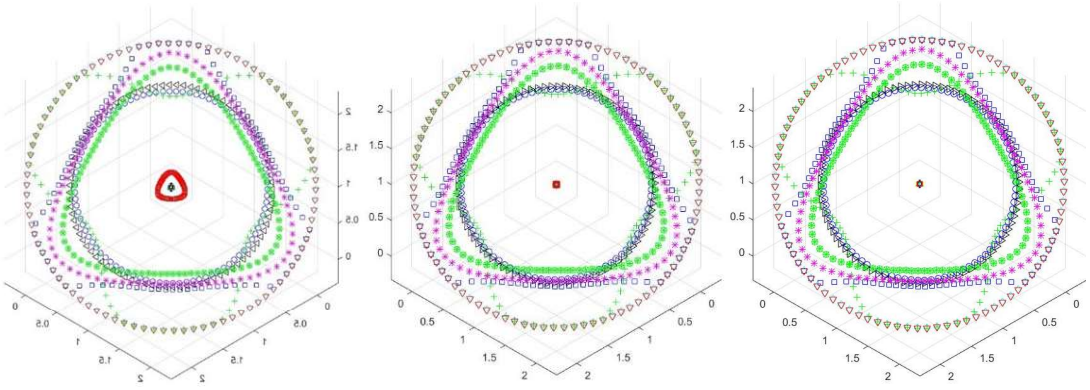

(a) (c) (e)

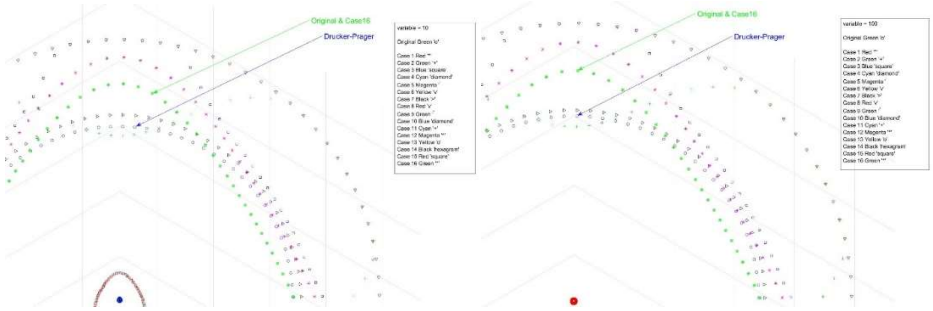

(b) (d)

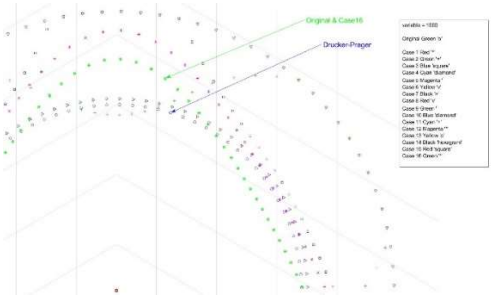

(f)

Figure 3-8(a)(b)(c)(d)(e)(f) illustration of sixteen cases on the π-plane with (a)(b) Δ=10, (c)(d) Δ=100, (e)(f) Δ=1000 (exponential relation).

In addition, case 2 and 3 are both out of shape and cases 1,4, 7, 8, 12 and 16 are particularly captivating. In figure 3-8(b)(d)(f), case 4, 7 and 8 are presented as a cycle, just like the small blue rings i.e. Drucker-Prager yield surface. From these three cases, case 7 is the closest one to the Drucker-Prager yield criterion, and it slightly approaching the Drucker-Prager yield surface during the value of Δ is tenfold increasing each condition. Case 4 and 8 matches well under three Δ initial conditions, and displays as cyan rhombus and red inverted triangle, respectively. The shapes of these two cases are the same as the Drucker-Prager one but are much bigger than it and they are over-predicted than original case hypoplastic yield surface in table 3-3. And it keeps the original shape of the yield surface (table 3-3) in case 1,12 and 16. Here, case 12 is a little over-predicting which is compared with the original hypoplastic one. Note that, from case 1 and 16, it can be concluded that there is no shape transformation existed if all four $C_i, i = 1,2,3,4$ are multiplied at the same time with the same variable Δ. It shows that the red '*', the green '*' and the green 'o' are coincided in figure 3.8(b)(d)(f) with three different variables Δ.

Therefore, an empirical conclusion can be made as that it is effectively to multiple C_1 and C_2 and multiple C_3 and C_4 with a different number at the same time. This result also coincides the concept of hypoplasticity which is separating the constitutive equation into two part linear and non-linear part. Summarizing the results aforementioned, the parameters $C_i, i = 1,2,3,4$ can be generated as follow,

Table 3-5 Parameters of material constants for matched hypoplastic Lade-Duncan and Hypoplastic Matsuoka-Nakai

	C_1	C_2	C_3	C_4
Lade-Duncan	-8.95	-80.15	-79.71	107.77
Matsuoka-Nakai	-87	-801.5	-797.1	1250

As shown in table 3-5, these two groups of parameters are generated from the $C_i, i = 1,2,3,4$ in table 3-3 [9]. Some traces can be dimly tracked that parameters above are calculated by the conclusion aforementioned e.g. ${C_2}^{LD} = {C_2}^{MN}/10$. With doing multiple and addition operation, two constitutive models are obtained with corresponding constants and can be plotted as figure 3-9(a) & (b). Here, Drucker-Prager yield criterion is denoted with blue rings, Lade-Duncan is black rings, Matsuoka-Nakai is the red one and two hypoplastic yield surfaces are displayed with green and cyan rings. It is obviously that all four yield surfaces are calibrated well at the point which represents the pure compression or so-called the point Lode angle equal zero.

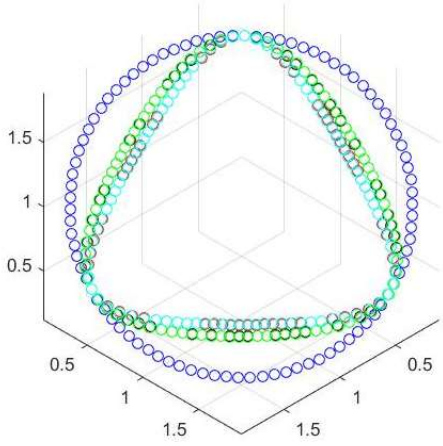

(a)

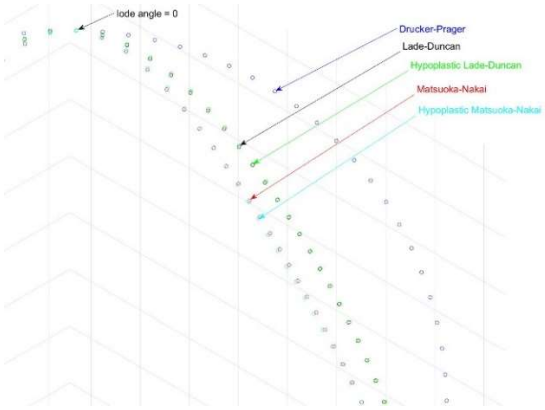

(b)

Figure 3-9(a)(b) Hypoplastic Lade-Duncan and Hypoplastic Matsuoka-Nakai yield surface matched with original Drucker-Prager, Lade-Duncan and Matsuoka-Nakai yield surface

The hypoplastic Lade-Duncan yield surface (Green one) matched with original Lade-Duncan one (Black one) well in figure 3-9(b) but is slightly over-predicting the strength. In contrast, the shape of the hypoplastic Matsuoka-Nakai is a little bit smaller than the original one.

4 PARAMETER STUDY WITH DEM TRUE-TRIAXIAL TEST

The improved hypoplastic yield surface introduced in chapter 3 has developed the hypoplastic Lade-Duncan and Matsuoka-Nakai yield surfaces which were matched the elastoplastic ones in [10] well, with two groups of parameters $C_i, i = 1,2,3,4$. But these parameters were totally obtained through the empirical method. As already mentioned in lots of article about hypoplastic constitutive model e.g. [11], it says that the dimensionless material parameters can be calibrated with triaxial compression test in [13]. In order to investigate a more accurate explanation of the parameters $C_i, i = 1,2,3,4$, the study will be discussed in this chapter with introducing the DEM true-triaxial test data in [10] and the procedures are shown as table 4-1.

Table 4-1 Flow chart for the parameter study with the DEM true-triaxial test.

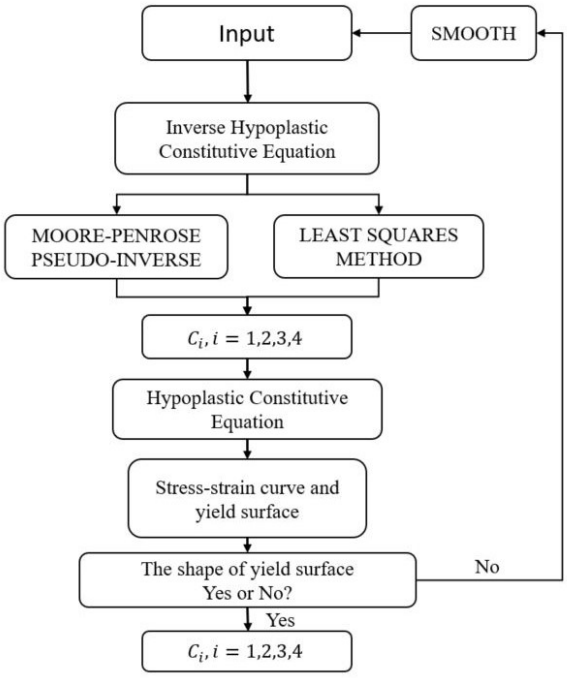

4.1 DEM true-triaxial test

The DEM true-triaxial test is processed based on the concept which is mentioned in [10] that the micromechanical phenomena have been illustrated in Figure 4-1(p.11 in [10]).

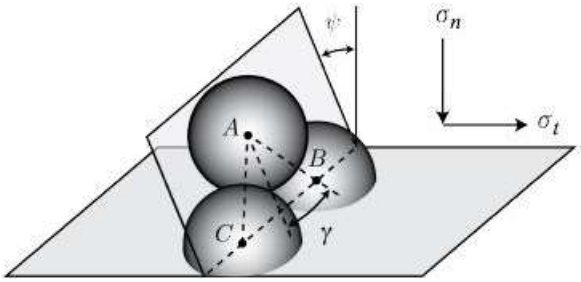

Figure 4-1(a) Three dimensional micromechanical effects involving inter-particle contact and motion on macro-scale slip plane. [10] The effects have been analyzed in detail in [19]

These true-triaxial DEM simulations were performed on the assemblies of about 3000-30000 mono-disperse spheres. Controlled by the strain paths $\dot{\varepsilon}_1, \dot{\varepsilon}_2, \dot{\varepsilon}_3$, where $\dot{\varepsilon}_1 + \dot{\varepsilon}_2 + \dot{\varepsilon}_3 = 0$, the test devotes to measure (principal) stresses corresponding to Lode angles varying between $0 \leq \alpha \leq 60^o$ in roughly 4^o increments (similar with table3-2). Otherwise, six randomly packed specimens were assigned uniform inter-particle friction coefficients ranging between $0.01 \leq \mu_{micro} \leq 0.8$ and particle rotation was also included in the simulation but would not be introduced in the hypoplastic constitutive model, due to the elimination of rotation tensor W which was aforementioned in chapter 3.3.1. [10] Here, 108 yield surfaces were obtained via the DEM true-triaxial simulation in [20,21]. The DEM simulations were performed using a modified version of the open-source codes LAMMPS (Large-scale Atomic/Molecular Massively Parallel Simulator) [22,23] and its derivative

LIGGGHTS (LAMMPS Improved for General Granular Heat Transfer Simulation) [24,25], with post-processing performed with the open-source code ParaView [26,27]. [10]

As the result of the DEM simulation, there are 9 cases which was substituted three different μ into three specimens showed in table 4-2. And each case has sixteen assemblies of strain rate respectively. All these outputs will be set up as the input of the hypoplastic parameter study in the later section.

Table 4-2 Three specimens combined with three different μ.

Specimen	$\mu = 0.2$	$\mu = 0.5$	$\mu = 0.8$
Specimen 4	Case1	Case2	Case3
Specimen 5	Case4	Case5	Case6
Specimen 6	Case7	Case8	Case9

Furthermore, the same true-triaxial simulation process can be applied on assemblies of poly-disperse spheres. As shown in figure 4-2, the assembly of 125000 spherical particles is considered here. And spheres consist with four different diameters specimens which is $\mathrm{d} = \{0.3,0.4,0.6,0.8\}$ mm, with a log-normal particle size distribution corresponding to ASTM C 778-06 standard well-graded (Ottawa) sand, with $d_{50} \approx 0.35\ mm$. (p.15 in [10]) The density of the sphere is $\rho = 3000\ kg/m^3$ (for quartz) and the inter-particle Coulomb friction coefficient $\mu_{micro} = 0.5$ (specially for dry quartz-on-quartz contact). And the initial yield ratio of the specimen was about $e \approx 0.66$, which corresponds to the initial volume density can be denoted as $v = 1/(1+e) \approx 0.6$. And the side length of initial cubical assembly of spheres as figure 4-2 was roughly 1.9 cm. Described in [21], the inter-particle rolling friction was not included, and tangential sliding

was computed using the true tangential displacement history contact model detailed in [28,29]. Any other parameters which was used in the DEM simulation can be referenced in [30].

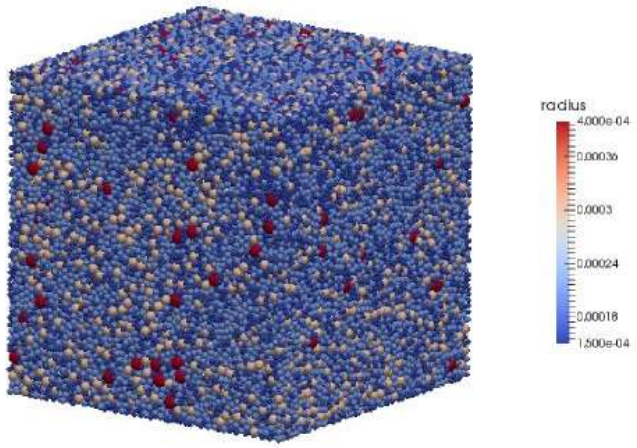

Figure 4-2 125000-sphere cubical DEM specimen for true-triaxial test simulation. (p.15 in [10])

Otherwise, the initial setting of the 125000-spheres DEM simulation which corresponds assemblies of poly-disperse spheres is shown in the table 4-3. The result of the true-triaxial DEM simulation which will be used in the later section is in term of the length of each side and the force in the three-dimension at each time step.

Table 4-3 Five strain rate combinations were applied in true-triaxial test simulation with 125000-sphere cubical DEM specimen, ($\dot{\varepsilon}_i$, λ and α were mentioned in chapter3.1.2).

	$\dot{\varepsilon}_1$	$\dot{\varepsilon}_2$	$\dot{\varepsilon}_3$	λ	α
(1)	$-0.05\ s^{-1}$	$-0.05\ s^{-1}$	$0.1\ s^{-1}$	$-1/2$	0^o
(2)	$-0.075\ s^{-1}$	$-0.025\ s^{-1}$	$0.1\ s^{-1}$	$-1/4$	16^o
(3)	$-0.1\ s^{-1}$	$0\ s^{-1}$	$0.1\ s^{-1}$	0	30^o
(4)	$-0.1\ s^{-1}$	$0.025\ s^{-1}$	$0.075\ s^{-1}$	$1/3$	44^o

(5)	$-0.1\ s^{-1}$	$0.05\ s^{-1}$	$0.05\ s^{-1}$	1	60^{o}

4.2 Parameter of hypoplastic constitutive model study

Here, as aforementioned in chapter 3.3.1, the equation 3-10 is introduced as the hypoplastic constitutive model which will be generated in this section. It can be rewritten as the tensor version as follow,

$$\dot{T}_{11} = C_1(trT)D_{11} + C_2\frac{tr(TD)}{tr(T)}T_{11} + C_3\frac{\sqrt{trD^2}}{tr(T)}{T_{11}}^2 + C_4\frac{\sqrt{trD^2}}{trT}({T_{11}}^*)^2 \text{----------(4-1)}$$

$$\dot{T}_{22} = C_1(trT)D_{22} + C_2\frac{tr(TD)}{tr(T)}T_{22} + C_3\frac{\sqrt{tr\ ^2}}{tr(T)}{T_{22}}^2 + C_4\frac{\sqrt{trD^2}}{trT}({T_{22}}^*)^2 \text{----------(4-2)}$$

$$\dot{T}_{33} = C_1(trT)D_{33} + C_2\frac{tr(TD)}{tr(T)}T_{33} + C_3\frac{\sqrt{trD^2}}{tr(T)}{T_{33}}^2 + C_4\frac{\sqrt{trD^2}}{trT}({T_{33}}^*)^2 \text{----------(4-3)}$$

As the original definition of the hypoplastic constitutive equation, C_i is regarded as the initial constants, stress *T* and logarithmic strain rates *D* are the inputs and stress rate $\dot{T}$ is considered as the output. In contrast, in order to investigate the value of the non-dimensional material parameter i.e. $C_i, i = 1,2,3,4$, stress *T*, logarithmic strain rates *D* and the stress rate $\dot{T}$ should be reversely regarded as the input. Then, the question can be viewed as the linear equation with four variables. Inspire by the method which was used in [31], Wu. W and Erich Bauer set up two equation (as equation 4-4, 5) which was applied on initial condition for the triaxial test as the table 4-4.

Table 4-4 Expressions of stress, strain rate, stress rate and spin tensors for triaxial test in [31].

Notion	σ	$\dot{\varepsilon}$	$\dot{\sigma}$	$\dot{\omega}$
Triaxial test	$\begin{pmatrix}\sigma_1 & 0 & 0\\ 0 & \sigma_3 & 0\\ 0 & 0 & \sigma_3\end{pmatrix}$	$\begin{pmatrix}\varepsilon_1 & 0 & 0\\ 0 & \varepsilon_3 & 0\\ 0 & 0 & \varepsilon_3\end{pmatrix}$	$\begin{pmatrix}\dot{\sigma}_1 & 0 & 0\\ 0 & \dot{\sigma}_3 & 0\\ 0 & 0 & \dot{\sigma}_3\end{pmatrix}$	$\begin{pmatrix}0 & 0 & 0\\ 0 & 0 & 0\\ 0 & 0 & 0\end{pmatrix}$

Note that, Wu and Bauer use the different notations in [31], but the same version of hypoplastic constitutive equation. Four linear equations were generated to calculate the parameters C_i with equation 4-4&5 which applied with two group of data from the triaxial test in table 4-4.

$$\dot{\sigma}_1 = C_1(\sigma_1 + 2\sigma_3)\dot{\varepsilon}_1 + C_2\frac{\sigma_1\dot{\varepsilon}_1+2\sigma_3\dot{\varepsilon}_3}{\sigma_1+2\sigma_3}\sigma_1 + \left[C_3{\sigma_1}^2 + \frac{4}{9}C_4(\sigma_1-\sigma_3)^2\right]\frac{\sqrt{{\dot{\varepsilon}_1}^2+2{\dot{\varepsilon}_3}^2}}{\sigma_1+2\sigma_3} \text{ ----------}$$

(4-4)

$$\dot{\sigma}_3 = C_1(\sigma_1 + 2\sigma_3)\dot{\varepsilon}_3 + C_2\frac{\sigma_1\dot{\varepsilon}_1+2\sigma_3\dot{\varepsilon}_3}{\sigma_1+2\sigma_3}\sigma_3 + \left[C_3{\sigma_3}^2 + \frac{1}{9}C_4(\sigma_1-\sigma_3)^2\right]\frac{\sqrt{{\dot{\varepsilon}_1}^2+2{\dot{\varepsilon}_3}^2}}{\sigma_1+2\sigma_3} \text{ ----------}$$

-(4-5)

Therefore, the equations can be set up as follow, where x_{ij} and Y_{ii} $i\&j = 1,2,3,4$, and these factors will all be the input from the results of DEM simulation.

$$C_1x_{11} + C_2x_{12} + C_3x_{13} + C_4x_{14} = Y_{11} \text{ ----------(4-6)}$$

$$C_1x_{21} + C_2x_{22} + C_3x_{23} + C_4x_{24} = Y_{22} \text{ ----------(4-7)}$$

$$C_1x_{31} + C_2x_{32} + C_3x_{33} + C_4x_{34} = Y_{33} \text{ ----------(4-8)}$$

$$C_1x_{41} + C_2x_{42} + C_3x_{43} + C_4x_{44} = Y_{44} \text{ ----------(4-9)}$$

Then, to eliminate C_1, equation 4-6,7,8,9 can be rearranged as equation 4-10,11,12,13.

$$x_{11}C_1 = Y_1 - x_{12}C_2 - x_{13}C_3 - x_{14}C_4$$ ----------(4-10)

$$x_{21}C_1 = Y_2 - x_{11}C_2 - x_{11}C_3 - x_{11}C_4$$ ----------(4-11)

$$x_{31}C_1 = Y_3 - x_{11}C_2 - x_{11}C_3 - x_{11}C_4$$ ----------(4-12)

$$x_{41}C_1 = Y_4 - x_{11}C_2 - x_{11}C_3 - x_{11}C_4$$ ----------(4-13)

Let the equation 4-11 be divided by 4-10 and the same as (4-11)/ (4-12) and (4-12)/ (4-13), then, the equation 4-14, 4-15 and 4-16 can be generated respectively.

$$(x_{11}/x_{21}) * (\mathrm{Y}_2 - x_{22}C_2 - x_{23}C_3 - x_{24}C_4) = \mathrm{Y}_1 - x_{12}C_2 - x_{13}C_3 - x_{14}C_4$$ ----------

(4-14)

$$(x_{31}/x_{41}) * (\mathrm{Y}_4 - x_{42}C_2 - x_{43}C_3 - x_{44}C_4) = \mathrm{Y}_3 - x_{32}C_2 - x_{33}C_3 - x_{34}C_4$$ ----------

(4-15)

$$(x_{21}/x_{31}) * (\mathrm{Y}_3 - x_{32}C_2 - x_{33}C_3 - x_{34}C_4) = \mathrm{Y}_2 - x_{22}C_2 - x_{23}C_3 - x_{24}C_4$$ ----------

(4-16)

It is necessary to factorize three equations above as the standard version (such as equation 4-6),

$$(x_{12} - \frac{x_{11}}{x_{21}} * x_{22})C_2 + (x_{13} - \frac{x_{11}}{x_{21}} * x_{23})C_3 + (x_{14} - \frac{x_{11}}{x_{21}} * x_{24})C_4 = Y_1 - \frac{x_{11}}{x_{21}}Y_2$$----------

(4-17)

$$(x_{22} - \frac{x_{21}}{x_{31}} * x_{32})C_2 + (x_{23} - \frac{x_{21}}{x_{31}} * x_{33})C_3 + (x_{24} - \frac{x_{11}}{x_{21}} * x_{34})C_4 = Y_2 - \frac{x_{21}}{x_{31}}Y_3$$----------

(4-18)

$$(x_{32}-\frac{x_{31}}{x_{41}}*x_{42})C_2+(x_{33}-\frac{x_{31}}{x_{41}}*x_{43})C_3+(x_{34}-\frac{x_{31}}{x_{41}}*x_{44})C_4=\ Y_3-\frac{x_{31}}{x_{41}}Y_4\text{----------}$$

(4-19)

and rearrange three equations as follow.

$$(x_{12}-\frac{x_{11}}{x_{21}}*x_{22})C_2=Y_1-\frac{x_{11}}{x_{21}}Y_2-(x_{13}-\frac{x_{11}}{x_{21}}*x_{23})C_3-(x_{14}-\frac{x_{11}}{x_{21}}*x_{24})C_4\text{---------(4-}$$

20)

$$(x_{22}-\frac{x_{21}}{x_{31}}*x_{32})C_2=Y_2-\frac{x_{21}}{x_{31}}Y_3-(x_{23}-\frac{x_{21}}{x_{31}}*x_{33})C_3-(x_{24}-\frac{x_{11}}{x_{21}}*x_{34})C_4\text{---------(4-}$$

21)

$$(x_{32}-\frac{x_{31}}{x_{41}}*x_{42})C_2=Y_3-\frac{x_{31}}{x_{41}}Y_4-(x_{33}-\frac{x_{31}}{x_{41}}*x_{43})C_3-(x_{34}-\frac{x_{31}}{x_{41}}*x_{44})C_4\text{---------(4-}$$

22)

Let the equation 4-21 be divided by 4-20 and the same as (4-21)/ (4-22), then, the equation 4-23 and 4-24 can be generated, respectively.

$$\frac{\left(x_{12}-\frac{x_{11}}{x_{21}}*x_{22}\right)}{\left(x_{22}-\frac{x_{21}}{x_{31}}*x_{32}\right)}*\left[Y_2-\frac{x_{21}}{x_{31}}Y_3-\left(x_{23}-\frac{x_{21}}{x_{31}}*x_{33}\right)C_3-\left(x_{24}-\frac{x_{11}}{x_{21}}*x_{34}\right)C_4\right]=$$

$$\left[Y_1-\frac{x_{11}}{x_{21}}Y_2-\left(x_{13}-\frac{x_{11}}{x_{21}}*x_{23}\right)C_3-\left(x_{14}-\frac{x_{11}}{x_{21}}*x_{24}\right)C_4\right]\text{-----(4-23)}$$

$$\frac{\left(x_{22}-\frac{x_{21}}{x_{31}}*x_{32}\right)}{\left(x_{32}-\frac{x_{31}}{x_{41}}*x_{42}\right)}*\left[Y_3-\frac{x_{31}}{x_{41}}Y_4-(x_{33}-\frac{x_{31}}{x_{41}}*x_{43})C_3-(x_{34}-\frac{x_{31}}{x_{41}}*x_{44})C_4\right]=$$

$$\left[Y_2-\frac{x_{21}}{x_{31}}Y_3-\left(x_{23}-\frac{x_{21}}{x_{31}}*x_{33}\right)C_3-(x_{24}-\frac{x_{11}}{x_{21}}*x_{34})C_4\right]\text{-----(4-24)}$$

Equation 4-23 and 4-24 are factorized as follow,

$$\left\{(x_{13}-\frac{x_{11}}{x_{21}}*x_{23})-\frac{\left(x_{12}-\frac{x_{11}}{x_{21}}*x_{22}\right)}{\left(x_{22}-\frac{x_{21}}{x_{31}}*x_{32}\right)}*(x_{23}-\frac{x_{21}}{x_{31}}*x_{33})\right\}*C_3=Y_1-\frac{x_{11}}{x_{21}}Y_2-$$

$$\frac{\left(x_{12}-\frac{x_{11}}{x_{21}}*x_{22}\right)}{\left(x_{22}-\frac{x_{21}}{x_{31}}*x_{32}\right)}*\left(Y_2-\frac{x_{21}}{x_{31}}Y_3\right)+\left\{\frac{\left(x_{12}-\frac{x_{11}}{x_{21}}*x_{22}\right)}{\left(x_{22}-\frac{x_{21}}{x_{31}}*x_{32}\right)}*\left(x_{24}-\frac{x_{11}}{x_{21}}*x_{34}\right)-\left(x_{14}-\frac{x_{11}}{x_{21}}*x_{24}\right)\right\}*$$

$$C_4 \text{ -----(4-25)}$$

$$\left\{\left(x_{23}-\frac{x_{21}}{x_{31}}*x_{33}\right)-\frac{\left(x_{22}-\frac{x_{21}}{x_{31}}*x_{32}\right)}{\left(x_{32}-\frac{x_{31}}{x_{41}}*x_{42}\right)}*\left(x_{33}-\frac{x_{31}}{x_{41}}*x_{43}\right)\right\}*C_3=Y_2-\frac{x_{21}}{x_{31}}Y_3-$$

$$\frac{\left(x_{22}-\frac{x_{21}}{x_{31}}*x_{32}\right)}{\left(x_{32}-\frac{x_{31}}{x_{41}}*x_{42}\right)}*\left(Y_3-\frac{x_{31}}{x_{41}}Y_4\right)+\left\{\frac{\left(x_{22}-\frac{x_{21}}{x_{31}}*x_{32}\right)}{\left(x_{32}-\frac{x_{31}}{x_{41}}*x_{42}\right)}*\left(x_{34}-\frac{x_{31}}{x_{41}}*x_{44}\right)-\left(x_{24}-\frac{x_{11}}{x_{21}}*x_{34}\right)\right\}*$$

$$C_4 \text{ -----(4-26)}$$

Here, in order not to mess up, the equation 4-25 and 4-26 are simplified as equation 4-27 and 4-28, where A_1, A_2, B_1, B_2, D_1 and D_2 are used to replace the long terms in previous two equations.

$$A_1 * C_3 = D_1 + B_1 * C_4 \text{ -----(4-27)}$$

$$A_2 * C_3 = D_2 + B_2 * C_4 \text{ -----(4-28)}$$

Where $A_1=(x_{13}-\frac{x_{11}}{x_{21}}*x_{23})-\frac{\left(x_{12}-\frac{x_{11}}{x_{21}}*x_{22}\right)}{\left(x_{22}-\frac{x_{21}}{x_{31}}*x_{32}\right)}*(x_{23}-\frac{x_{21}}{x_{31}}*x_{33}), A_2=$

$$\left(x_{23}-\frac{x_{21}}{x_{31}}*x_{33}\right)-\frac{\left(x_{22}-\frac{x_{21}}{x_{31}}*x_{32}\right)}{\left(x_{32}-\frac{x_{31}}{x_{41}}*x_{42}\right)}*\left(x_{33}-\frac{x_{31}}{x_{41}}*x_{43}\right), B_1=\frac{\left(x_{12}-\frac{x_{11}}{x_{21}}*x_{22}\right)}{\left(x_{22}-\frac{x_{21}}{x_{31}}*x_{32}\right)}*$$

$$\left(x_{24}-\frac{x_{11}}{x_{21}}*x_{34}\right)-\left(x_{14}-\frac{x_{11}}{x_{21}}*x_{24}\right), B_2=\frac{\left(x_{22}-\frac{x_{21}}{x_{31}}*x_{32}\right)}{\left(x_{32}-\frac{x_{31}}{x_{41}}*x_{42}\right)}*\left(x_{34}-\frac{x_{31}}{x_{41}}*x_{44}\right)-$$

$\left(x_{24}-\frac{x_{11}}{x_{21}}*x_{34}\right), D_1 = Y_1 - \frac{x_{11}}{x_{21}}Y_2 - \frac{\left(x_{12}-\frac{x_{11}}{x_{21}}*x_{22}\right)}{\left(x_{22}-\frac{x_{21}}{x_{31}}*x_{32}\right)} * \left(Y_2 - \frac{x_{21}}{x_{31}}Y_3\right) and\ D_2 = Y_2 -$

$\frac{x_{21}}{x_{31}}Y_3 - \frac{\left(x_{22}-\frac{x_{21}}{x_{31}}*x_{32}\right)}{\left(x_{32}-\frac{x_{31}}{x_{41}}*x_{42}\right)} * \left(Y_3 - \frac{x_{31}}{x_{41}}Y_4\right).$

On solving all the equation above, the non-dimensional material parameter $C_i, i = 1,2,3,4$ can be summarized as the equation which are substituted with the stress, the logarithmic strain rates and the stress rate.

$$C_4 = \frac{A_1D_2 - A_2D_1}{A_2B_1 - A_1B_2} \text{ -----(4-29)}$$

$$C_3 = \frac{A_1B_1D_2 - A_1B_2D_1}{A_1A_2D_1 - A_1A_1B_2} \text{ -----(4-30)}$$

$$C_2 = \left(Y_1 - \frac{x_{11}}{x_{21}}Y_2 - (x_{13} - \frac{x_{11}}{x_{21}} * x_{23})C_3 - (x_{14} - \frac{x_{11}}{x_{21}} * x_{24})C_4\right) / \left(x_{12} - \frac{x_{11}}{x_{21}} * x_{22}\right) \text{ -----}$$

(4-31)

$$C_1 = (Y_1 - x_{12}C_2 - x_{13}C_3 - x_{14}C_4)/x_{11} \text{-----(4-32)}$$

But it is hard to solve the four variables problem with three equation such as equation 4-1,2 and 3. Therefore, the Moore-Penrose inverse method is introduced to solve this problem. Here, the matrix is considered to be generated as follow. Letting the factors of the forth lateral row of the tensor H be number 0, and the forth vertical factor be zero as well.

$$\text{H} = \begin{pmatrix} x_{11} & x_{12} & x_{13} & x_{14} \\ x_{21} & x_{22} & x_{23} & x_{24} \\ x_{31} & x_{32} & x_{33} & x_{34} \\ 0 & 0 & 0 & 0 \end{pmatrix} \text{----------(4-33)}$$

$$\text{T} = (Y_1 \quad Y_2 \quad Y_3 \quad 0)' \text{ -----(4-34)}$$

Then, with substituting the four by four matrix H and the four by one matrix T into equation 4-35 as follow, the four parameters can be obtained, where C is the four by one matrix. In addition, the least square method is used to obtain the unique matrix solution from the equation 4-35.

$$\mathrm{C} = H^{-1} * T \text{ ----------(4-35)}$$

In summary, all four parameters C_1, C_2, C_3 and C_4 can be obtained through solving the equation system above with inputting the result from the DEM true-triaxial test. Compared with the totally empirical method model in chapter 3, both can generate the non-dimensional material parameters C. However, the parameter obtained in chapter 4 is much more convictive because of they are generated from the actual triaxial test (DEM version). From lots of literature review, it is the only and the best method to get these material constants. The more concrete results will be displayed in chapter 5. Therefore, solving the improved hypoplastic constitutive model for the parameter calculation will tend to get the more accurate results C than the model in previous chapter.

5 Results and Discussion

This chapter presents results from the improved hypoplastic constitutive model, which incorporates the improved non-dimensional material parameters $C_i, i = 1,2,3,4$ obtained through the data from the DEM true-triaxial test. Both 3000-30000 mono-disperse spheres and 125000 spherical poly-disperse spheres are considered in the DEM true-triaxial test. Otherwise, comparison between the hypoplastic constitutive model with the old parameters and the model with the improved data will be displayed and will also be used to compare with the Lade-Duncan, Matsuoka-Nakai and Mohr-Coulomb yield surface which was shown in previous chapter.

5.1 3000-30000 mono-disperse spheres

The parameter C with three different mono-disperse particles under three μ conditions can be obtained by solving the inverse hypoplastic constitutive equation. And each condition was under sixteen combinations of initial strain rate in three-dimension which is shown in table5-1.

Table 5-1 Sixteen strain rate combinations with applied in true-triaxial test simulation with 3000-30000 mono-disperse spheres

media	$\dot{\varepsilon}_1$	$\dot{\varepsilon}_2$	$\dot{\varepsilon}_3$	media	$\dot{\varepsilon}_1$	$\dot{\varepsilon}_2$	$\dot{\varepsilon}_3$
1	0.005	0.005	-0.01	9	-0.005	-0.005	0.01
2	0.0057	0.0043	-0.01	10	-0.0057	-0.0043	0.01
3	0.0064	0.0036	-0.01	11	-0.0064	-0.0036	0.01
4	0.0071	0.0029	-0.01	12	-0.0071	-0.0029	0.01
5	0.0079	0.0021	-0.01	13	-0.0079	-0.0021	0.01

6	0.0086	0.0014	-0.01	14	-0.0086	-0.0014	0.01
7	0.0093	0.0007	-0.01	15	-0.0093	-0.0007	0.01
8	0.01	0	-0.01	16	-0.01	0	0.01

Then, 144 groups of non-dimensional material parameters C are generated through the method aforementioned in chapter4 with inputs which are 144 groups of results from DEM true-triaxial test. The group of parameter C is generated with the least square method, because of each time step will generate specific parameter C, which is totally useful to get the approximate the solution from the inverse hypoplastic constitutive equation system. Figure 5-1 shows the value of the non-dimensional material parameters C for specimen 4 in each case.

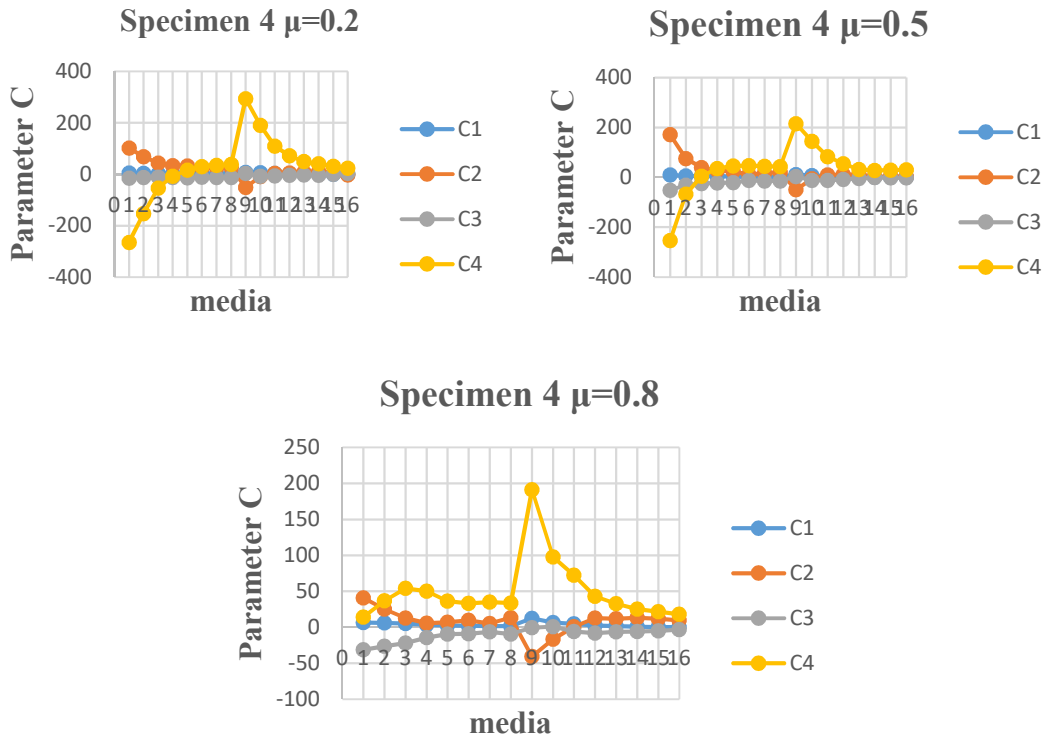

Figure 5-1. The parameter C for specimen 4 under μ = 0.2, 0.5, 0.8 with each media case. Here, C_1 is by blue curve, C_2, C_3 and C_4 are displayed by orange, gray and yellow, respectively.

It shows that each case has the similar variation tendency that C_1 is approximately similar to the straight line; C_2 decreases at the beginning and reaches the lowest point at media 9, then increases around the mid value; C_3 is similar as C_1 but it is easy to figure out that C_3 increases at beginning; C_4 increases at first and is stable around the mid value until case 9 point, then decrease and settles in the position where a little higher than the mid value. Here, the case which μ=0.8, is different with other two cases that C_4 start from the positive number and is always above the axis-x. Note that, media 1-8 should be totally opposite to the media 9-16.

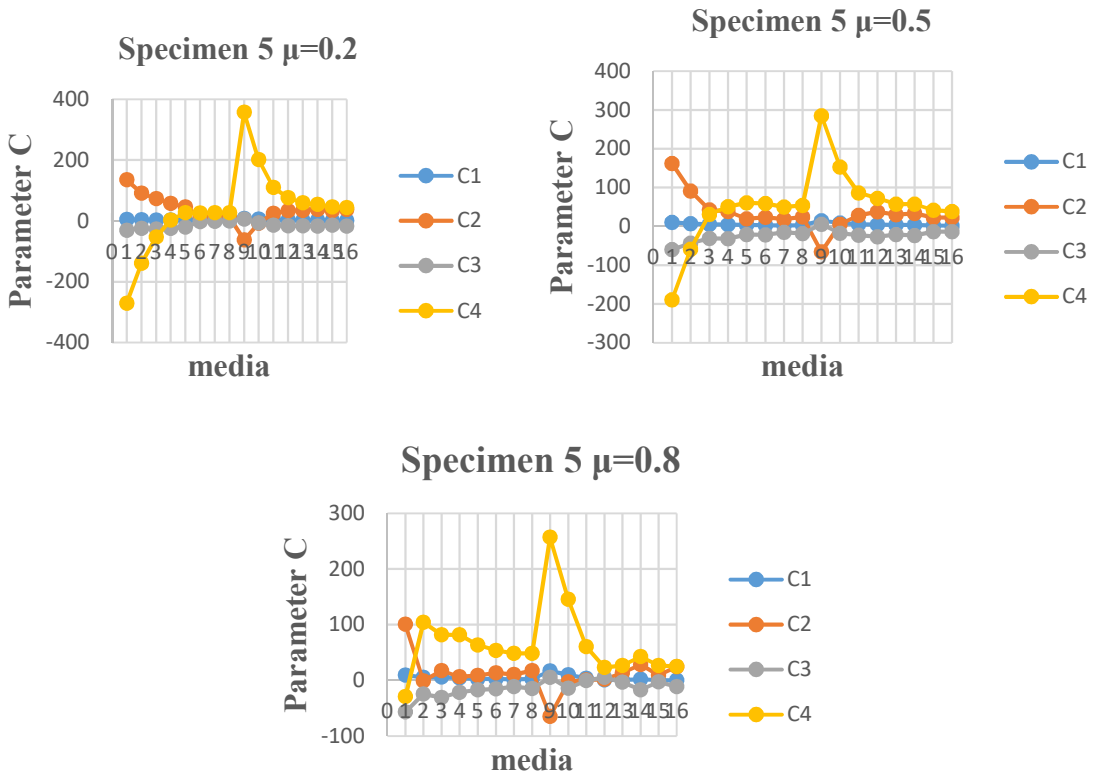

Figure 5-2. The parameter C for specimen 5 under μ = 0.2, 0.5, 0.8 with each media case. Here, C_1 is by blue curve, C_2, C_3 and C_4 are displayed by orange, gray and yellow, respectively.

Figure 5-2 shows the parameter value for specimen 5 in each case. It looks similar with the cases which were shown in figure 5-1 for specimen 4. Note that, it exists that some wave which was produced by some input error.

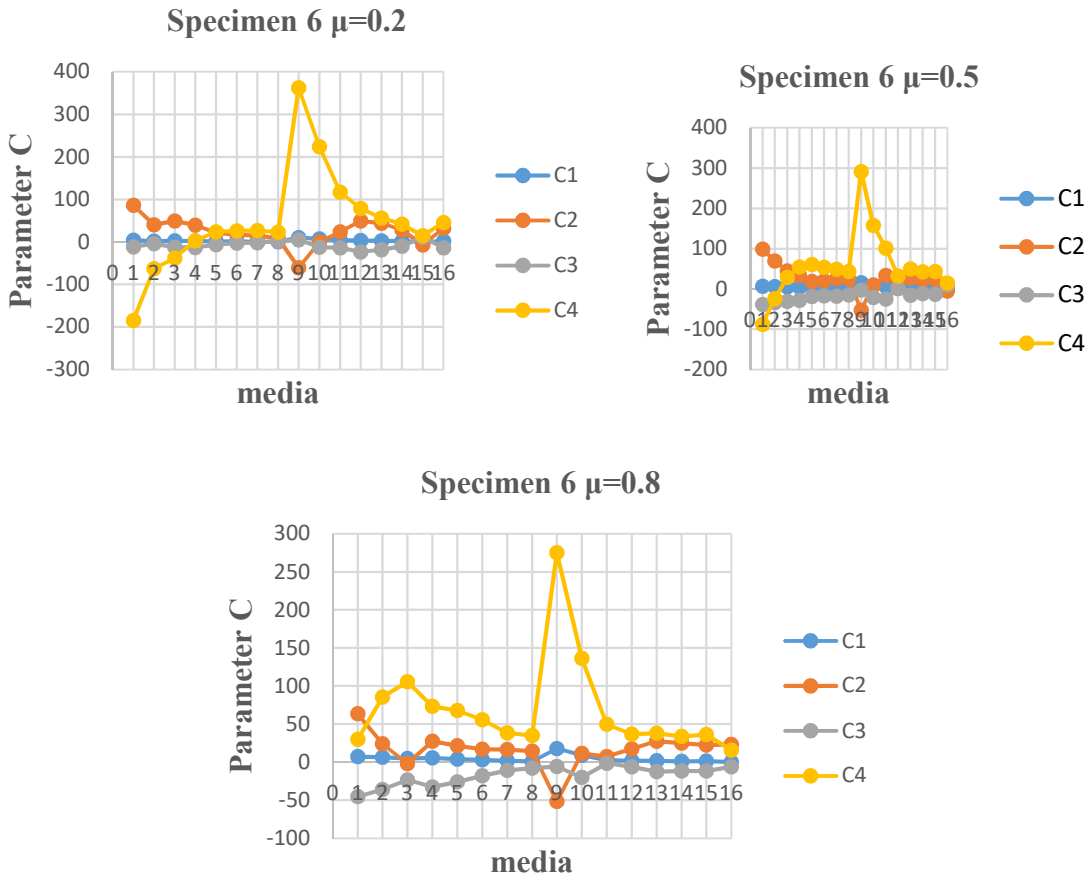

Figure 5-3. The parameter C for specimen 6 under μ = 0.2, 0.5, 0.8 with each media case. Here, C_1 is by blue curve, C_2, C_3 and C_4 are displayed by orange, gray and yellow, respectively.

Specimen 6's parameters looks like the same alignment as previous two specimens, but it's not hard to know that the value of C_4 at media 1 increases with the enhancement of

μ value. This phenomenon is the same with specimen 5, but not specimen 4. Note that, it is positive in compression.

Next step, all the parameter obtained above are substituted back to the model i.e. equation 4-1, 4-2, 4-3, as the non-dimensional material constants. Otherwise, the parameter C under each time step, will also be used to put back into the equation 4-1,4-2,4-3 which is useful to detect whether the parameter generated from inverse hypoplastic concept works or not. Note, the well-matched parameter C which was generated through the method mentioned in chapter 3 (begin with the number obtained from the DEM data) is concerned as well.

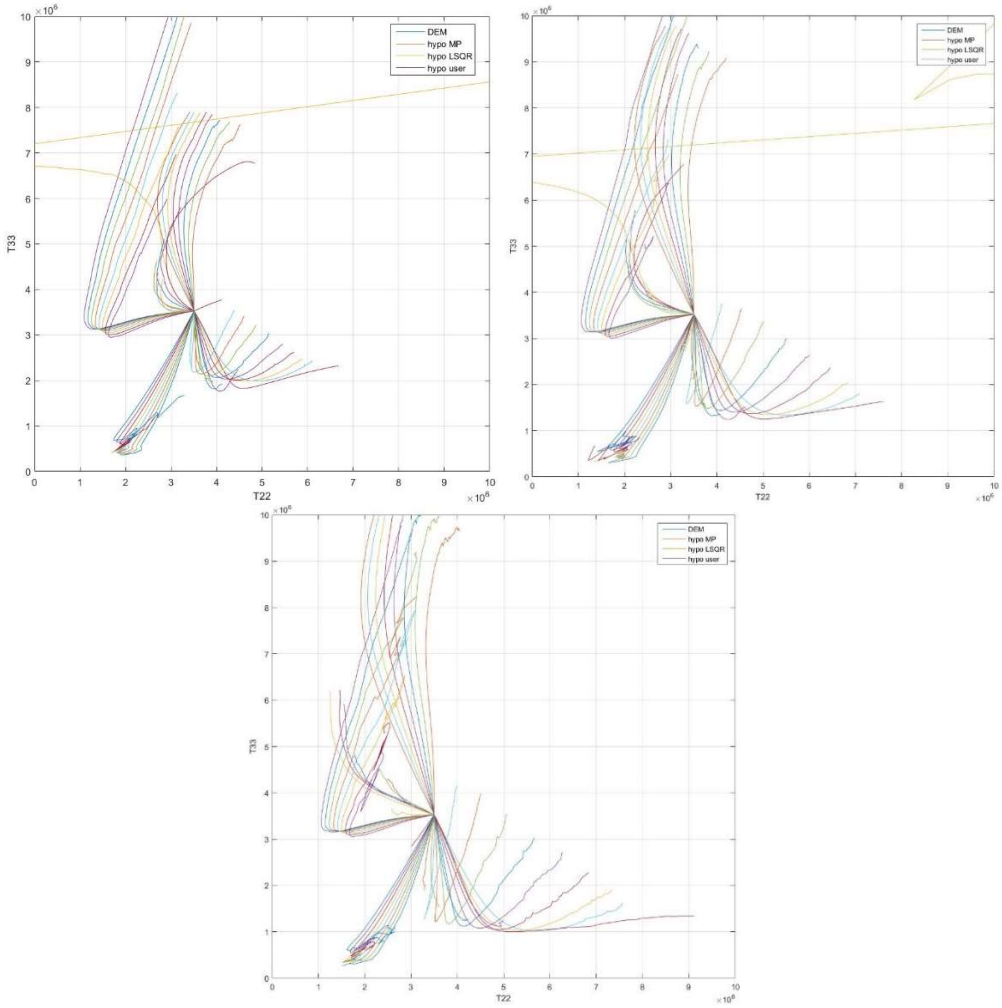

Figure 5-4 Stress path for Specimen 4 contained the DEM original, stress paths with each time step parameter C, re-substituted hypoplastic and well-matched constant C value. $\mu = 0.2,0.5,0.8$ (from upper left to lower one).

In figure 5-4 it shows the stress path in T_{11}-T_{22} dimension working with the specimen 4 under the initial conditions $\mu = 0.2,0.5,0.8$. The shape of the stress paths matched the generally shape of the stress paths, as the cone, but not totally coupling. It is clearly noticed that some data clutter exists in the DEM true-triaxial test value. Especially, the yellow curve which represented the media 1, displays the traceless shape, which not like the small wave (can be detected when zooming in). Coincided with the results discovered from figure 5-1, 5-2, 5-3, it can be easily found that C_2 and C_4 at media 1 point with $\mu = 0.2$ & 0.5, were far away from the intermediate value. Here, several reasons can be hypothesized, that the input data from DEM true-triaxial test was not stable or the least square method was not measured the relative accurate value. As the lower one in figure 5-4, the least square method generated the curve which was not traceless as upper two, the probability of the former reason is preferred in this chapter.

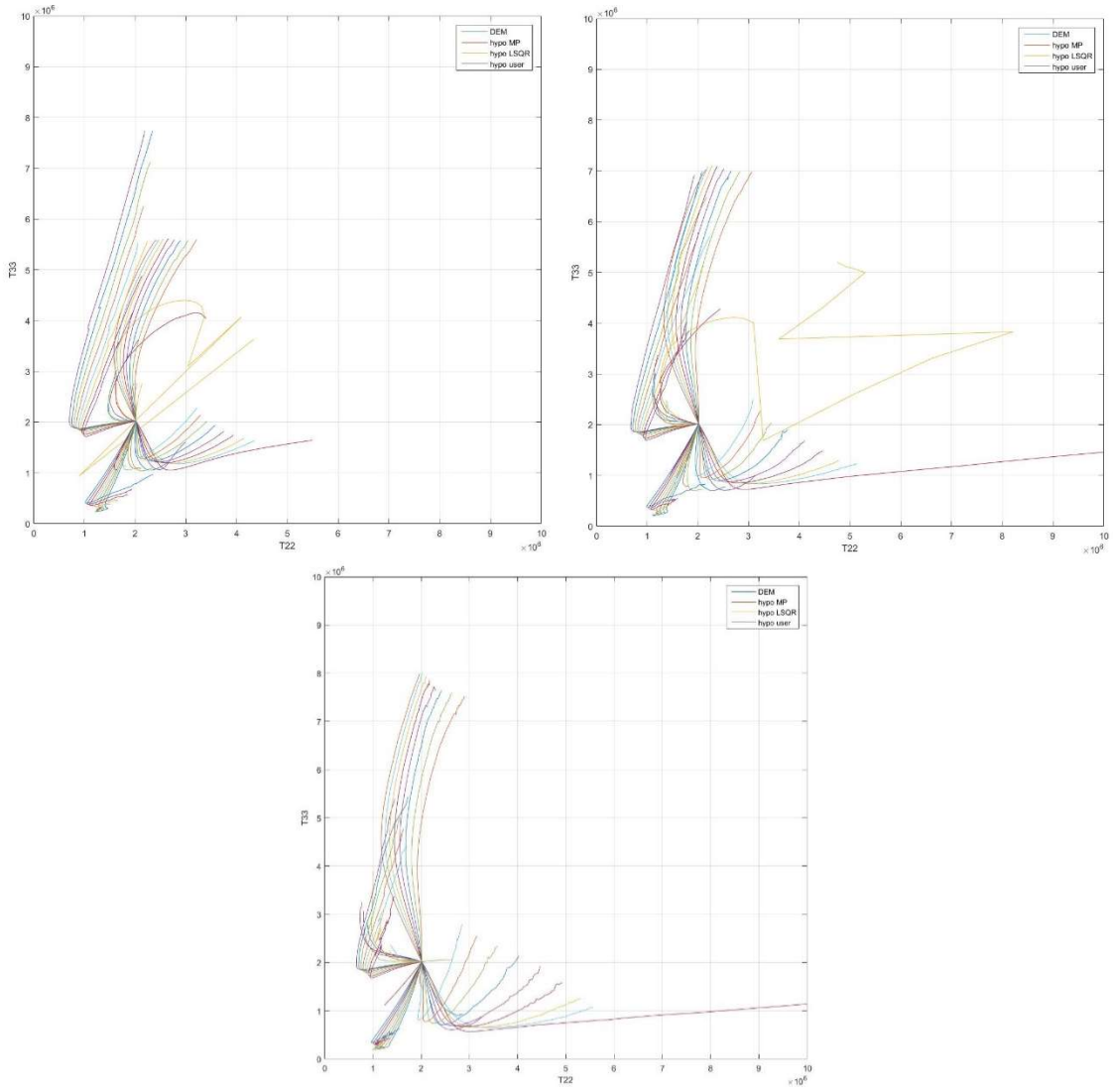

Figure 5-5 Stress path for Specimen 5 contained the DEM original, stress paths with each time step parameter C, re-substituted hypoplastic and well-matched constant C value. $\mu = 0.2,0.5,0.8$ (from upper left to lower one).

Same as specimen 4, specimen 5 plots the traceless curve when $\mu = 0.2$ & 0.5 at media 1 point and the curve under $\mu = 0.8$ is better. And it matches good at media 9 point for all the $\mu = 0.2,0.5,0.8$, even though lower and upper right curve in figure 5-5, it extends towards as the straight line. It can be imagined that the point on the curve media 9 is projected on the π-plane, will not be large deviation when compared with DEM yield

surface. The figure 5-6 shows the stress path for specimen 5 with $\mu = 0.5$ & 0.8 at media 9 point.

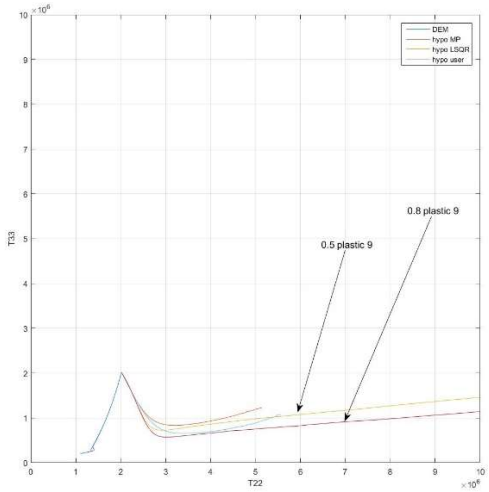

Figure 5-6 Stress path for Specimen 5 with $\mu = 0.5$ & 0.8 (media 9)

In figure 5-6, the cone whose $\mu = 0.8$ looks slightly bigger than the other. It seems that the yield starts earlier if μ is small.

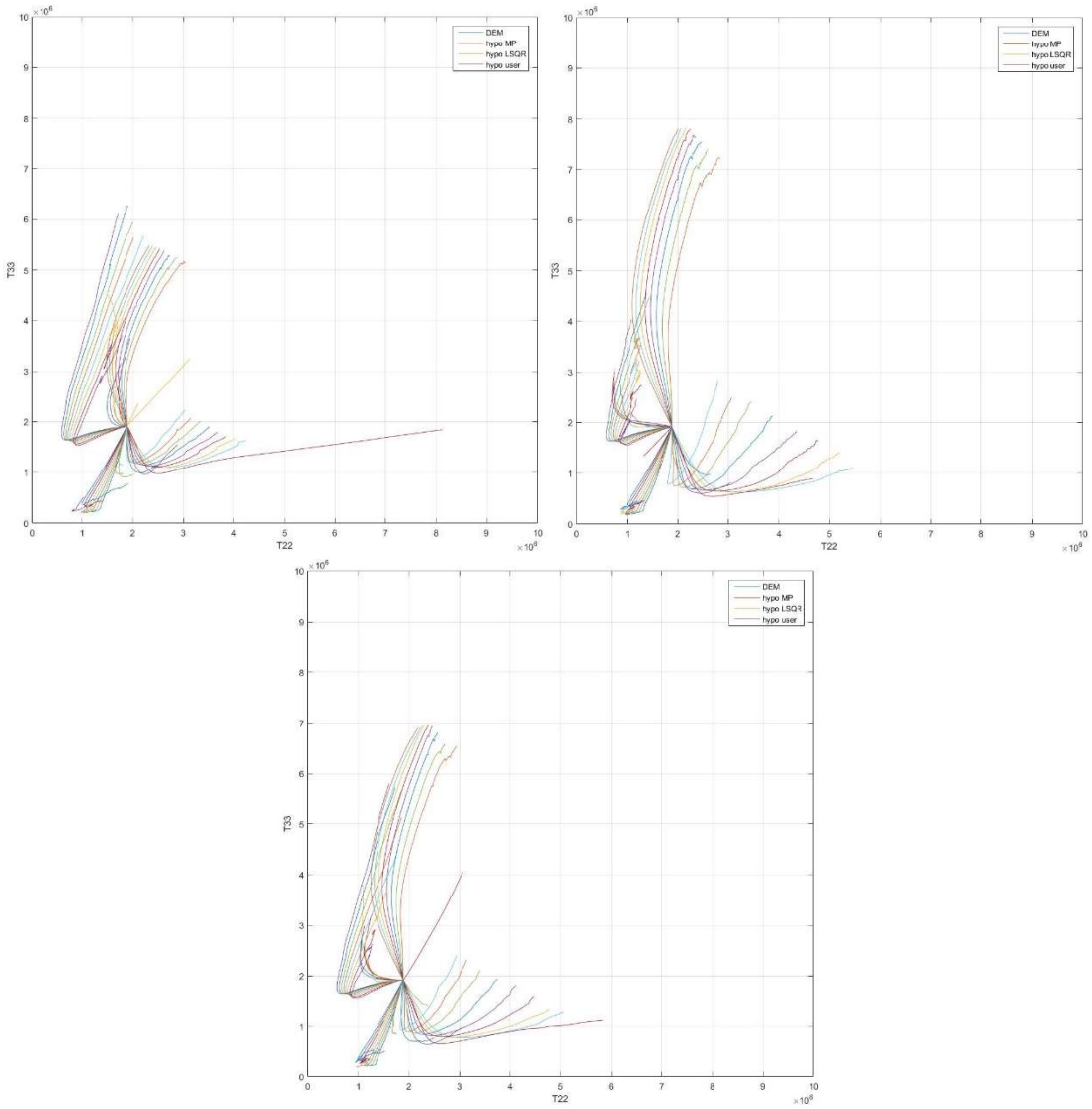

Figure 5-7 Stress path for Specimen 6 contained the DEM original, stress paths with each time step parameter C, re-substituted hypoplastic and well-matched constant C value. $\mu =$ 0.2,0.5,0.8 (from upper left to lower one).

In figure 5-7, same conclusions aforementioned in this chapter are also suitable for specimen 6.

From the visible outcome above, the available parameter C without data clutter, are collected. Then, all these parameters which are assumed useful, will be substituted into the hypoplastic yield model, i.e. equation 3-21, 3-22, 3-23.

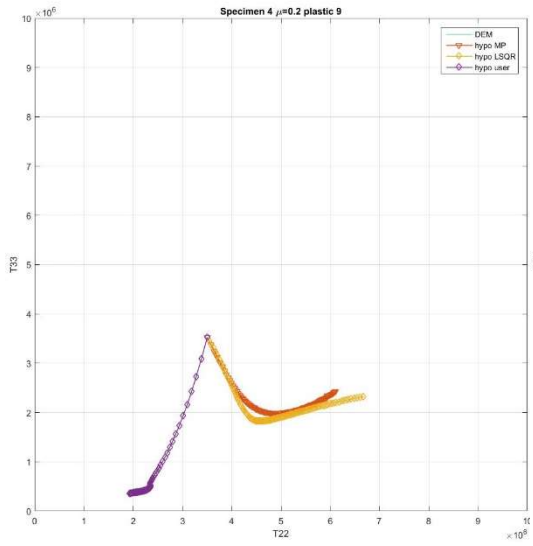
Specimen 4 μ=0.2 plastic 9
DEM
hypo MP
hypo LSQR
hypo user
T33
T22

(a)

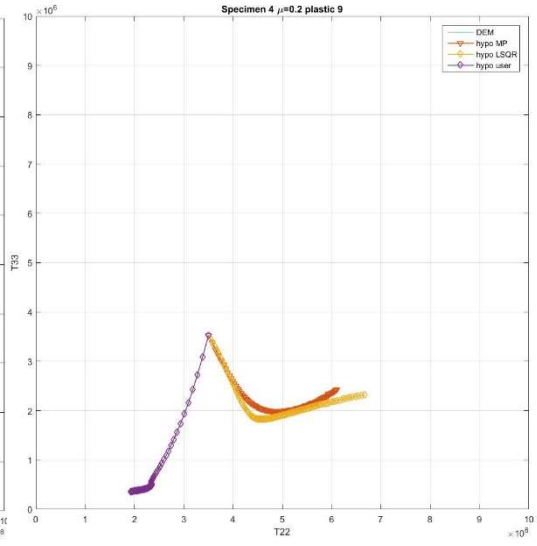
Specimen 4 μ=0.2 plastic 9
DEM
hypo MP
hypo LSQR
hypo user
T33
T22

(b)

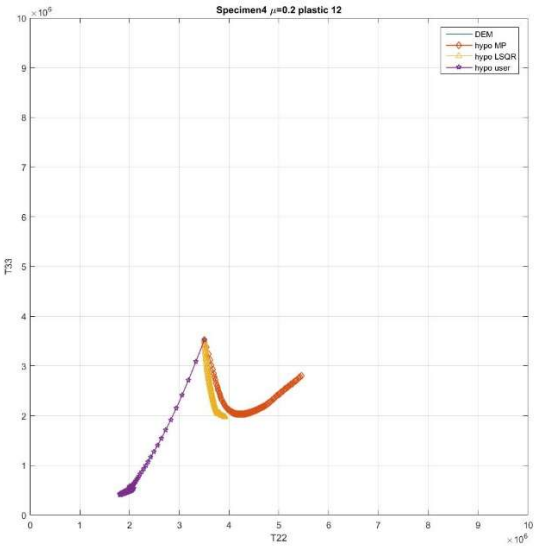
Specimen4 μ=0.2 plastic 12
DEM
hypo MP
hypo LSQR
hypo user
T33
T22

(c)

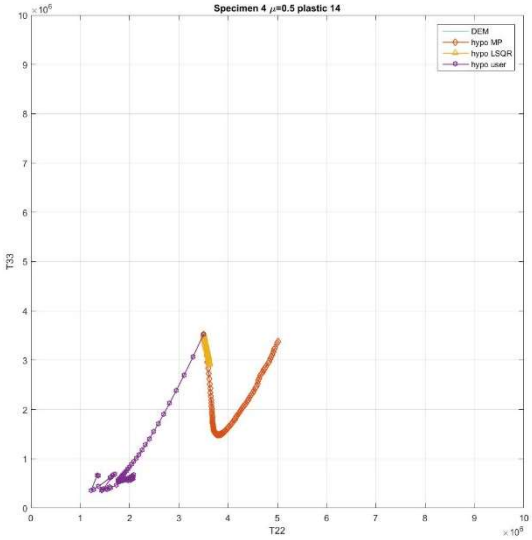
Specimen 4 μ=0.5 plastic 14
DEM
hypo MP
hypo LSQR
hypo user
T33
T22

(d)

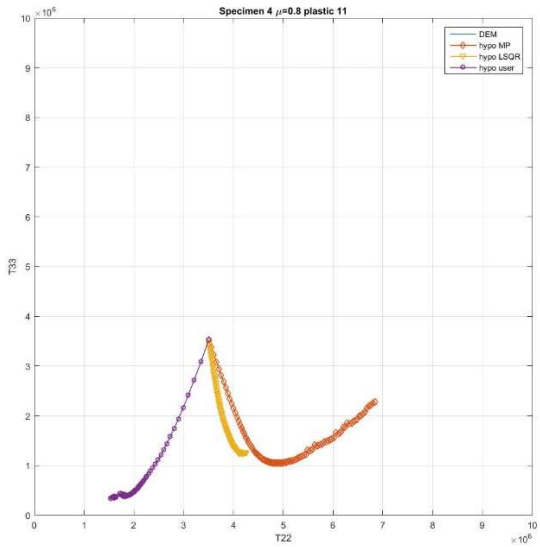

(e)

Figure 5-8 Stress paths for specimen 4 where (a) μ = 0.2 media 9 (b) μ = 0.2 media 11 (c) μ = 0.2 media 12 (d) μ = 0.5 media 14 (e) μ = 0.8 media 11

In terms of specimen 4, four cases showed in figure 5-8 are selected to re-input to the hypoplastic yield model. Similar with figure 5-6, figure 5-8 (a) and (b) showed that the hypoplastic curve is closed to the DEM curve which was coupling with the hypoplastic curve (each time rate) but corner part the DEM one is much smoother than hypoplastic did for each case (a) and (b). Other three ones are matching or close to the DEM curve which is the results from original true-triaxial test, e.g. (d) shows that the hypoplastic curve is coincided with the DEM one, but stop before the corner, and (c) and (e) are close to the curves from the test. And the value of parameter C is showed as follow, (a) $C_1 = 7.9274$, $C_2 = -51.2522$, $C_3 = 3.5784$, $C_4 = 293.9323$ (b) $C_1 = 3.6982$, $C_2 3.8184$, $C_3 = -6.5076$, $C_4 = 109.9211$ (c) $C_1 = 2.4662$, $C_2 = 5.6438$, $C_3 = -3.7731$, $C_4 = 72.0196$ (d) $C_1 = 0.6579$, $C_2 = 1.5587$, $C_3 = 0.1355$, $C_4 = 27.3685$ (e) $C_1 = 4.5526$, $C_2 = 0.9456$, $C_3 = -5.9557$, $C_4 = 72.5039$.

Then, the same steps will be processed as follow.

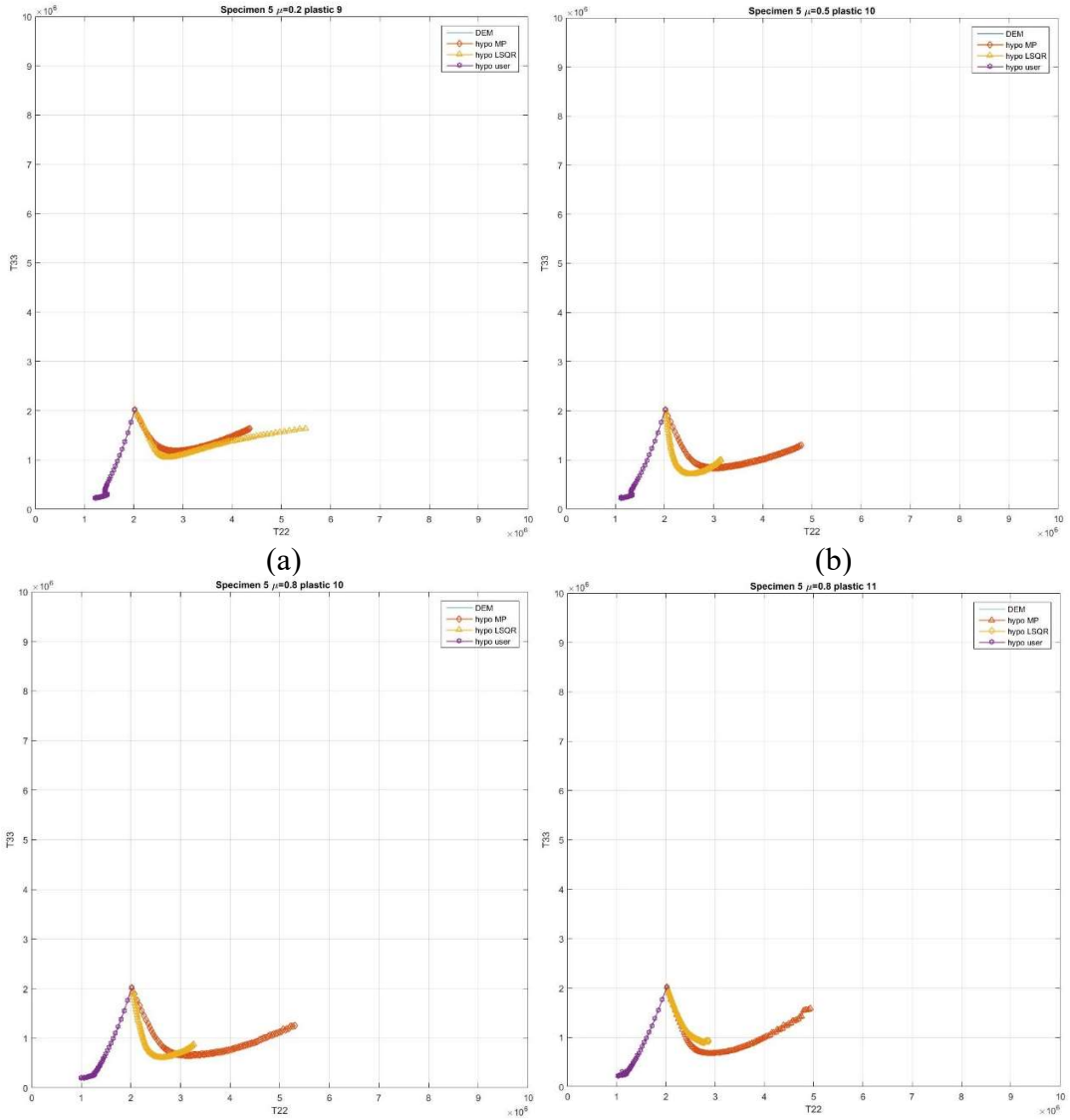

Figure 5-9 Stress paths for specimen 5 where (a) μ = 0.2 media 9 (b) μ = 0.5 media 10 (c) μ = 0.8 media 10 (d) μ = 0.8 media 11

In figure 5-9, the upper left one matches the best in all four cases for specimen 5, and the value of parameter C is as follow, (a) $C_1 = 9.9217, C_2 = -62.5279, C_3 = 6.0032, C_4 = 357.0266$ (b) $C_1 = 9.0349$, $C_2 = 5.8059$, $C_3 = -17.7538$, $C_4 = 152.786$ (c) $C_1 = 9.8768$, $C_2 = -2.6651$, $C_3 = -13.9561$, $C_4 = 145.5293$ (d) $C_1 = 3.4862$, $C_2 = 0.5534$, $C_3 = -0.4368, C_4 = 60.4213$.

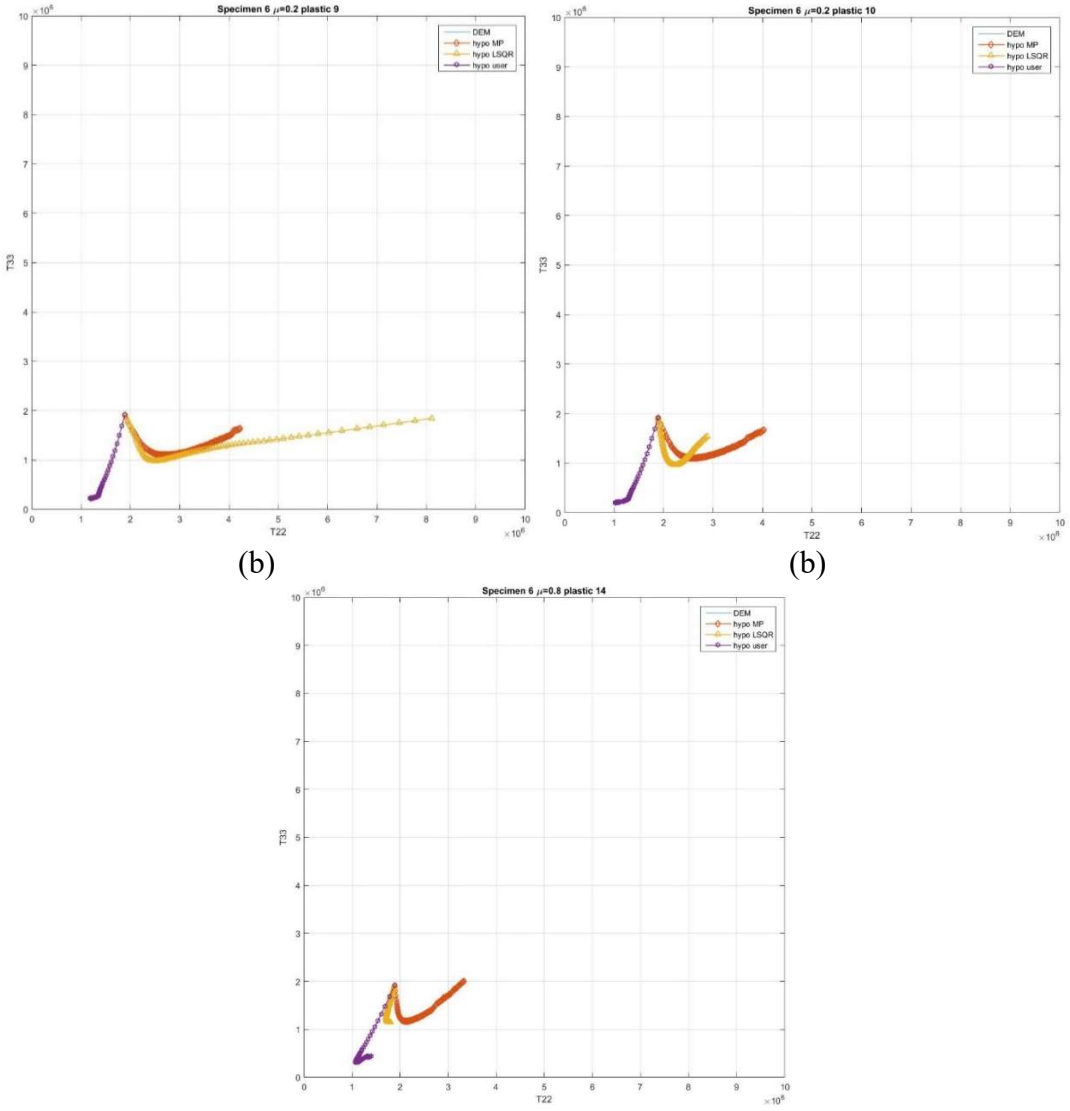

(b) (b)

(c)

Figure 5-10 Stress paths for specimen 5 where (a) μ = 0.2 media 9 (b) μ = 0.2 media 10 (c) μ = 0.8 media 14

According to specimen 6, three cases were picked and showed in figure 5-10. And parameter C for each case in figure 5-10 is as follow, (a) $C_1 = 10.2099, C_2 = -60.7115, C_3 = 4.5806, C_4 = 362.4224$ (b) $C_1 = 7.0528, C_2 = -0.6799, C_3 = -12.4261, C_4 = 223.9126$ (c) $C_1 = 1.1538, C_2 = 24.8831, C_3 = -11.7323, C_4 = 33.9546.$

As already grabbed from 144 cases of parameter C, these parameter C showed above will be substituted back to the hypoplastic yield model B.

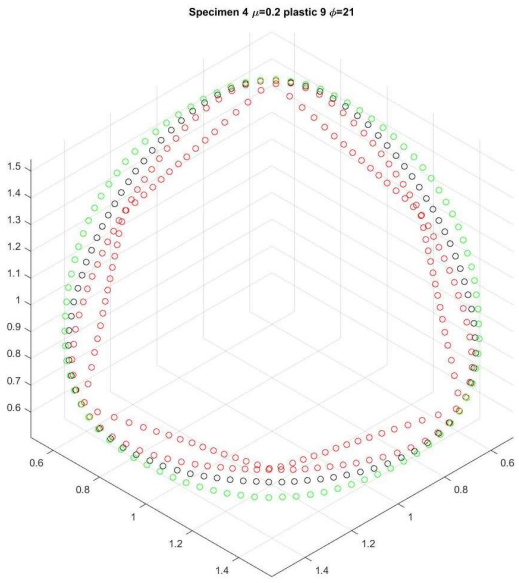
Specimen 4 μ=0.2 plastic 9 ϕ=21

(a)

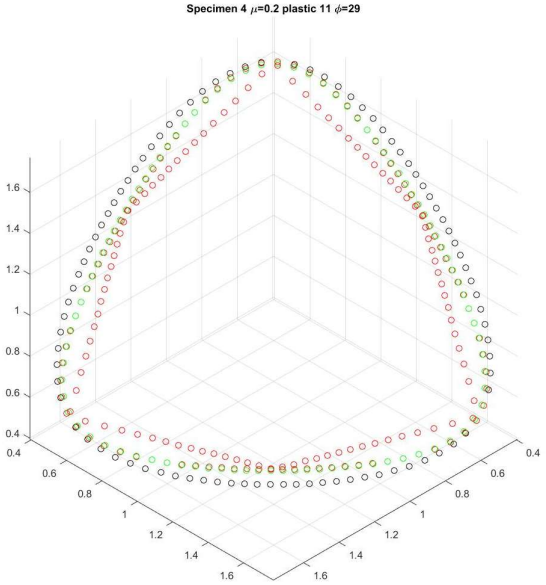
Specimen 4 μ=0.2 plastic 11 ϕ=29

(b)

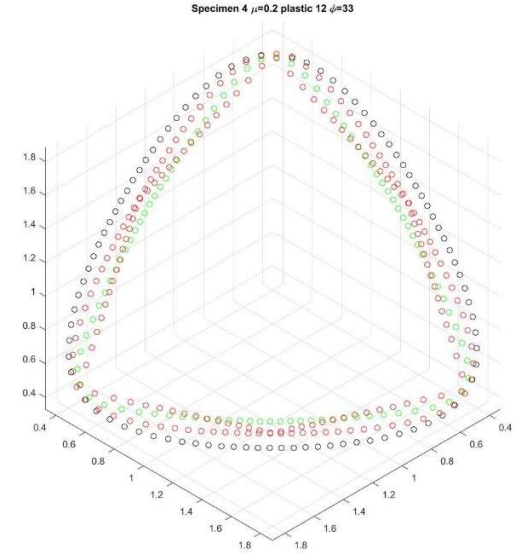
Specimen 4 μ=0.2 plastic 12 ϕ=33

(c)

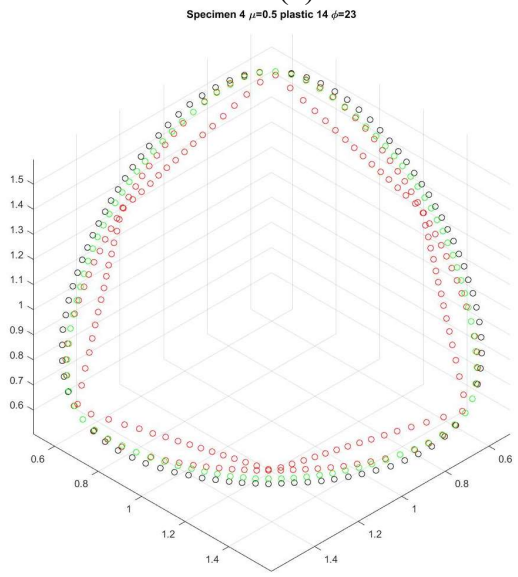
Specimen 4 μ=0.5 plastic 14 ϕ=23

(d)

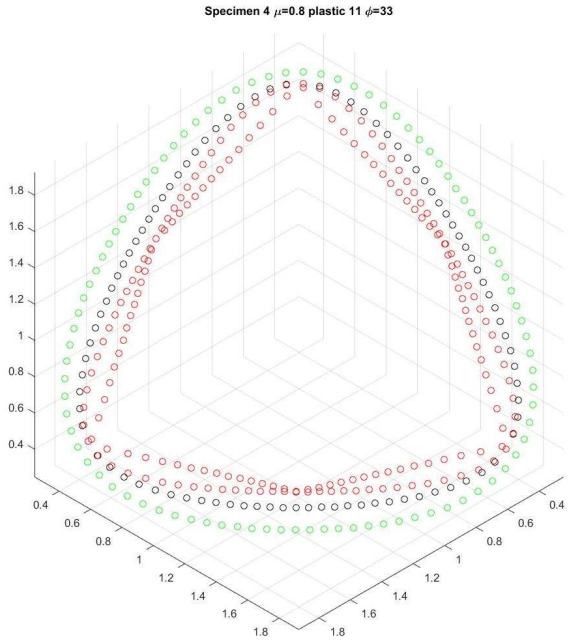

(e)

Figure 5-11 Hypoplastic yield surface in terms of specimen 4 with different non-dimensional material parameters $C_i, i = 1,2,3,4$ (a) $\mu = 0.2$ media 9 (b) $\mu = 0.2$ media 11 (c) $\mu = 0.2$ media 12 (d) $\mu = 0.5$ media 14 (e) $\mu = 0.8$ media 11, compared with Lade-Duncan, Matsuoka-Nakai and Mohr-Coulomb yield surface.

In figure 5-11a, hypoplastic yield surface calibrated to match the numerically determined yield surface in pure compression (lode angle equal 0), with φ = 21 where φ is the macro-scale friction angle. The shape of the hypoplastic yield surface is not the cycle which is not the Drucker-Prager yield surface (the shape is always displayed as a cycle on the π-plane) but over-predicts the strength for Lade-Duncan (black ring in the figure5-11) yield surface at the point (lode angle $\alpha = 60$, so-called pure extension). It shows that yield surfaces which corresponded with parameter C for cases (b), (c), (d) and (e), calibrated to match the other yield surface in vertex point with φ = 29, 33, 23 and 33 respectively. Here, in case (b), the hypoplastic yield surface match Matsuoka-Nakai yield surface; in case (c), the hypoplastic one match the pure compression point at the beginning and shrink very fast, that is known to under-predict the strength in pure extension point (compare with other

three yield criterion); in case (d) and (e), the hypoplastic yield surface are both close to Lade-Duncan curve by surprise (note that, figure 5-11e calibrated with $\varphi = 33$ due to the Mohr-Coulomb yield surface which will blow up if $\varphi > 34$).

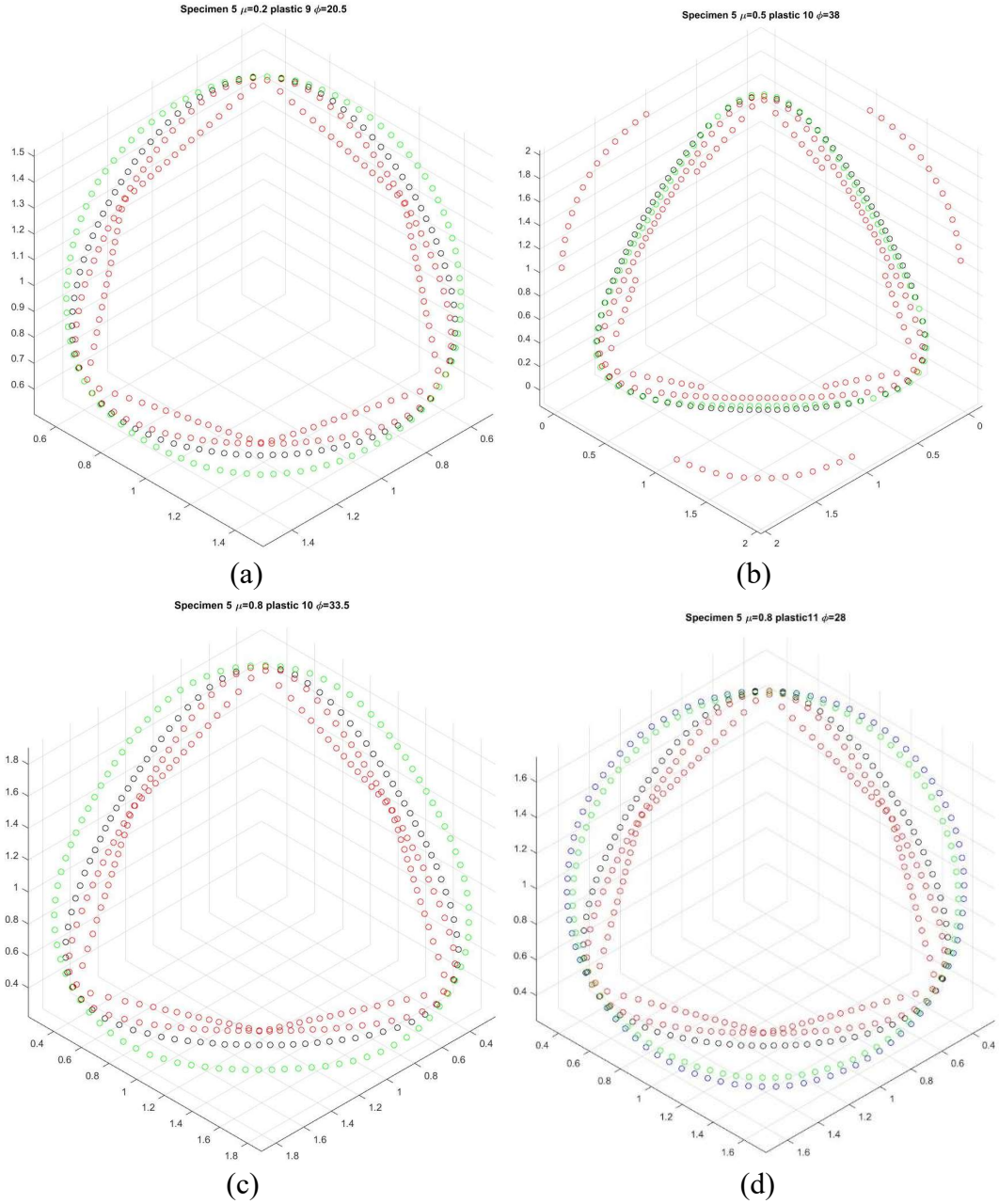

Figure 5-12 Hypoplastic yield surface in terms of specimen 5 with different non-dimensional material parameters $C_i, i = 1,2,3,4$ (a) $\mu = 0.2$ media 9 (b) $\mu = 0.5$ media 10 (c) $\mu = 0.8$ media 10 (d) $\mu = 0.8$ media 11, compared with Lade-Duncan,

Matsuoka-Nakai and Mohr-Coulomb yield surface (Drucker-Prager yield surface in d).

Figure 5-12 (a), (b), (c) and (d) show that hypoplastic yield surface was calibrated to coincide at a lode angle of $\alpha = 0$ with $\varphi = 20.5$, $\varphi = 38$, $\varphi = 33.5$ and $\varphi = 28$, respectively. Hypoplastic yield surfaces (a), (c) and (d) are over-predicted at the point where lode angle $\alpha = 60$(pure extension). Distinguishing from Drucker-Prager, the shape projected on the π-plane of all these three yield surfaces are not as simple as a cycle. Specially, the Drucker-Prager yield surface was considered in lower right figure to make the comparison with the hypoplastic one for $\mu = 0.8$ media 11. It is clear that the hypoplastic one is close to the Drucker-Prager but still not a perfect cycle. It is worth mentioning that in figure 5-12b, both the hypoplastic yield surface and Lade-Duncan one was coincided well not only at the calibrating point ($\alpha = 0$), but also the pure extension condition. Unfortunately, the Mohr-Coulomb yield surface was fitted when $\varphi = 38$. But it is obviously that hypoplastic yield surface matched the Lade-Duncan one but not the Matsuoka-Nakai one in this special case.

In a word, the two curves of hypoplastic yield surface and Lade-Duncan yield surface are closer to each other than other two curves for specimen 5 under each four conditions.

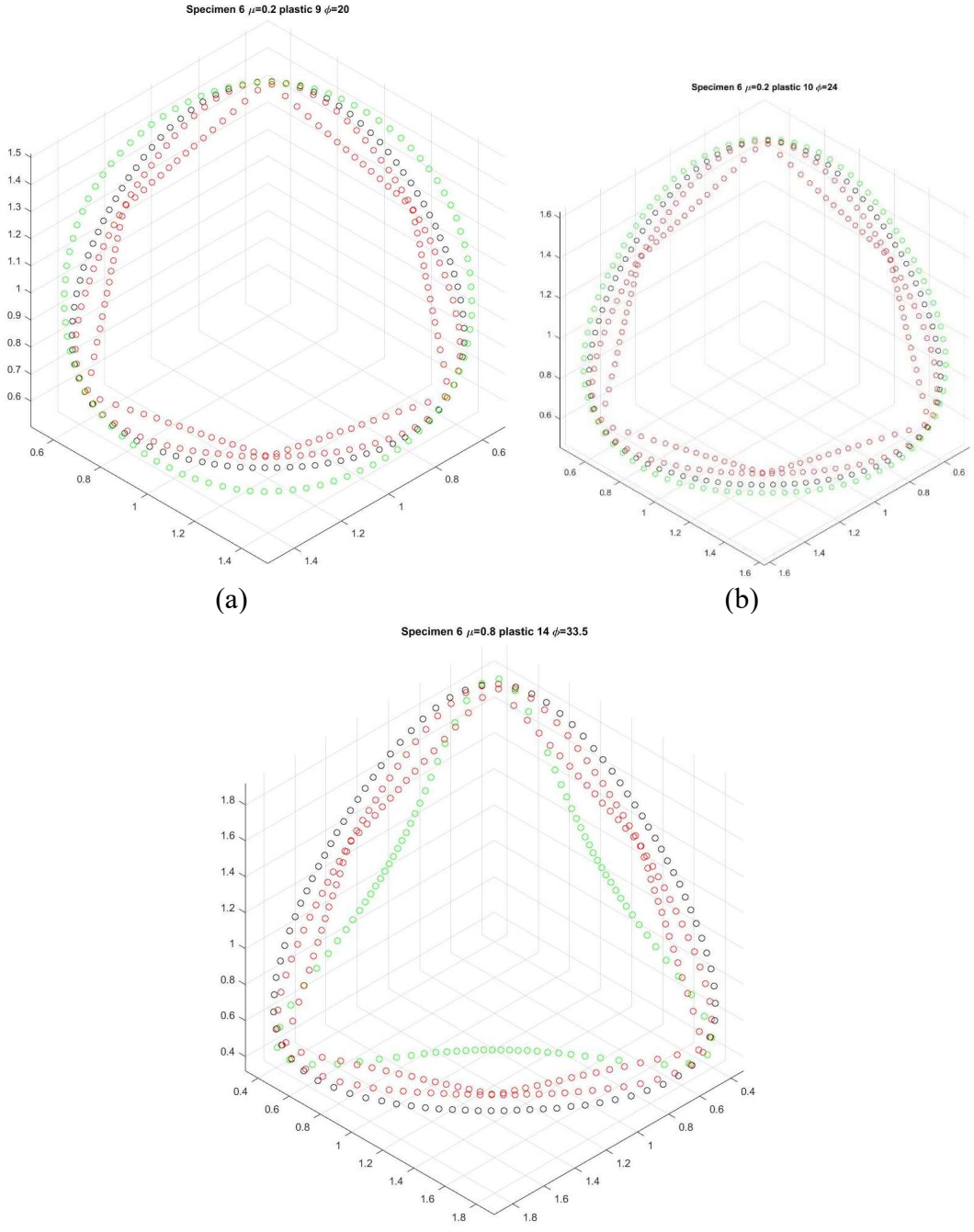

(a) (b)

(c)

Figure 5-13 Hypoplastic yield surface in terms of specimen 6 with different non-dimensional material parameters $C_i, i = 1,2,3,4$ (a) $\mu = 0.2$ media 9 (b) $\mu = 0.2$ media 10 (c) $\mu = 0.8$ media 14, compared with Lade-Duncan, Matsuoka-Nakai and Mohr-Coulomb yield surface.

Then, looking at the specimen 6, all four yield surfaces are calibrated to match at pure compression point with $\varphi = 20$, $\varphi = 24$ and $\varphi = 33.5$, respectively for each

condition in figure 5-13 (a)(b)(c). The curves in (a) and (b) are similar with the results in figure 5-12(a), (c) and (d) that both hypoplastic yield curves over-predict the strength of specimen 6 than Lade-Duncan (Matsuoka-Nakai and Mohr-Coulomb as well) but under-predict when compared with Drucker-Prager yield surface. And the lower case in figure 5-13, the shape of hypoplastic yield surface looks 'lanky' than any other yield surface (other hypoplastic yield surface which were generated in this paper are counted as well). It seems that the hypoplastic constitutive model for specimen 6 $\mu = 0.8$ media 14 is not as well as other two constitutive model which was showed in figure 5-10.

In sum, most of hypoplastic yield surfaces aforementioned which were substituted with non-dimensional material parameters $C_i, i = 1,2,3,4$ for 3000-30000 mono-disperse spheres are close to the Lade-Duncan yield curve (some of them are coincided well and the others are close and under-predict when match the Drucker-Prager one). But it still exists some unmatched yield surfaces and the stress path as well. Note that, all the results from the very early part of this section are substituted back to the hypoplastic yield model B, some of these hypoplastic yield surfaces which were not displayed in this paper coincide the Lade-Duncan yield surface well at pure extension point and also the point lode angle α near 60, but not match the general calibrating point. Due to this reason it is hard to estimate whether the hypoplastic yield surface are calibrated successfully or not. In order to fix these problems, some optimization will be processed in next section which will work with 125000 spherical poly-disperse spheres.

5.2 125000 spherical poly-disperse spheres

As already did in section 5.1, the same procedure will be operated in this section with the output from the DEM true-triaxial test for 125000 spherical poly-disperse spheres. The strain rate combinations for 125000 spherical poly-disperse spheres which will be applied to the reverse hypoplastic model are displayed in table 5-2.

Table 5-2 Seven strain rate combinations with applied in true-triaxial test simulation with 125000 spherical poly-disperse spheres.

Lode angle	$\dot{\varepsilon}_1$	$\dot{\varepsilon}_2$	$\dot{\varepsilon}_3$
0	-0.001	-0.001	0.002
10	-0.0005	-0.0015	0.002
20	0	-0.002	0.002
30	0.00025	-0.002	0.00175
40	0.0005	-0.002	0.0015
50	0.00075	-0.002	0.00125
60	0.001	-0.002	0.001

Then, seven groups of non-dimensional material parameters $C_i, i = 1,2,3,4$ are generated from seven samples for seven cases in table 5-2. All seven groups of parameter C are presented as follow.

Table 5-3 Seven groups non-dimensional material parameters $C_i, i = 1,2,3,4$

Lode angle	C_1	C_2	C_3	C_4
0	2.1279	53.8426	-55.918	395.0334
10	3.9597	93.7937	-49.1817	132.5976

20	3.2384	83.3375	-35.9898	91.7782
30	3.2366	81.8352	-32.4868	90.8295
40	4.1385	97.4922	-40.1754	112.7138
50	5.3817	75.2097	-32.7274	189.6429
60	16.5304	-6.9414	-36.5571	746.5925

By comparing with the parameter C which was obtained from the DEM true-triaxial test for 3000-30000 mono-disperse spheres, C_1, C_2, C_3 and C_4 displayed in table 5-3 become much more stable that C_1, C_2 and C_3 do not fluctuate greatly, but C_4 decreases from a large number in the beginning and goes up to a big value (nearly twice as large as the number at lode angle equal 0). The fluctuation of the value of parameter C will be visually to display with the figure as follow.

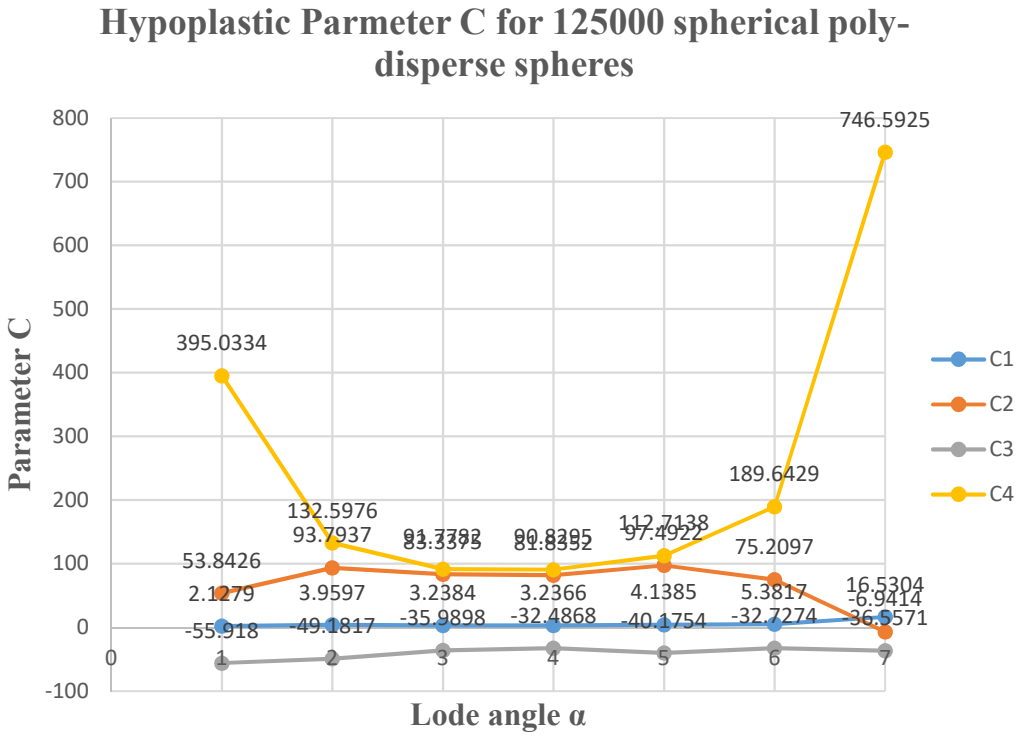

Figure 5-14 The parameter C for 125000 spherical poly-disperse spheres

In figure 5-14, it is clear that both cures for C_2 and C_4 are not as gently as the curves for C_1 and C_3. And it is not fit that the description of the input which is that the same material with same parameter (not like the input in section 5.1 that nine samples contained different material behaviors) should generate the material parameter such as C_1 and C_3 in figure 5-14.

In order to fix the problem above, the input data which was obtained from the DEM true-triaxial test for 125000 spherical poly-disperse spheres should be optimized. Through the MATLAB code for smoothing noise data, the optimized data is showed as follow.

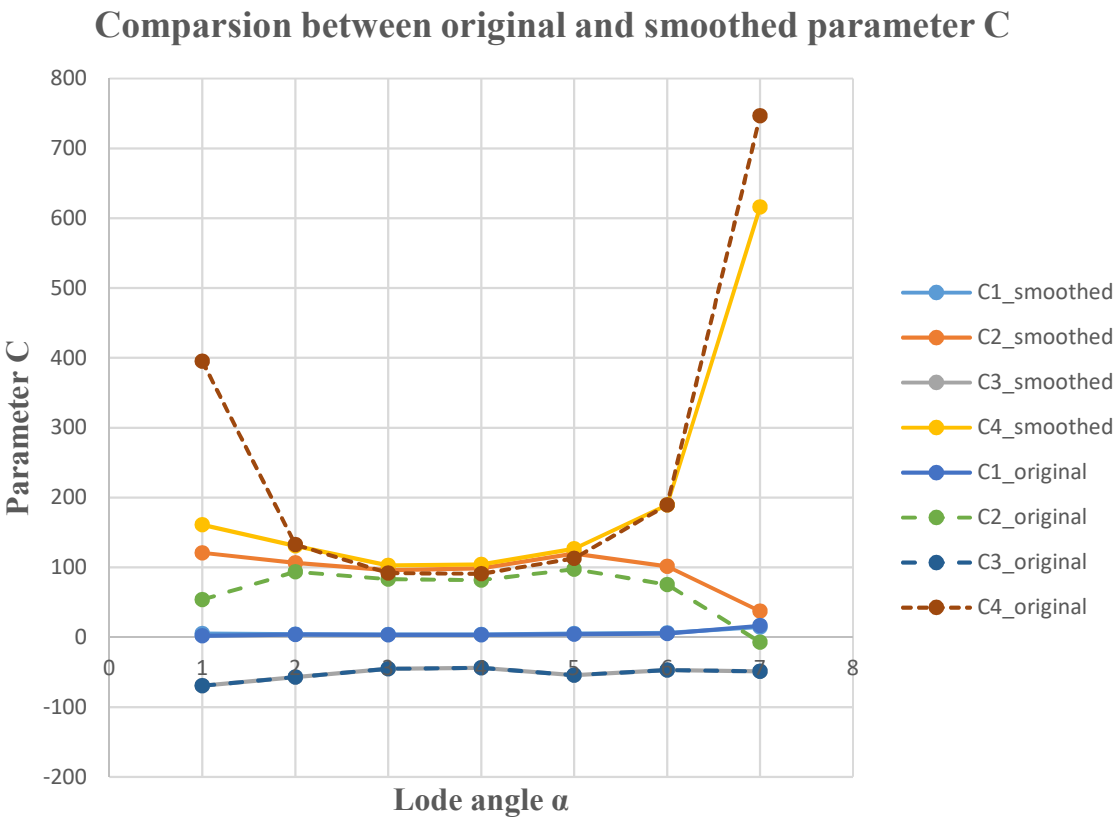

Figure 5-15 The parameter C for 125000 spherical poly-disperse spheres both smoothed (solid line) and the original (dotted line)

It can be easily found that the data for smoothed C_1 and C_3 are nearly the same as the original ones, and C_2 and C_4 are better than the raw results. Especially C_2, in figure 5-15, the curve for C_2 do not sharp ups and downs as before. And the point in C_4 curve for lode angle equal zero is not as higher as the point (dotted line) in original C_4 curve in the beginning; therefore, the point in C_4 curve for lode angle equal sixty is smaller than the original one.

Then, both the previous generated parameter C and the smoothed parameter C will be substituted into both the hypoplastic constitutive equation and the yield equation.

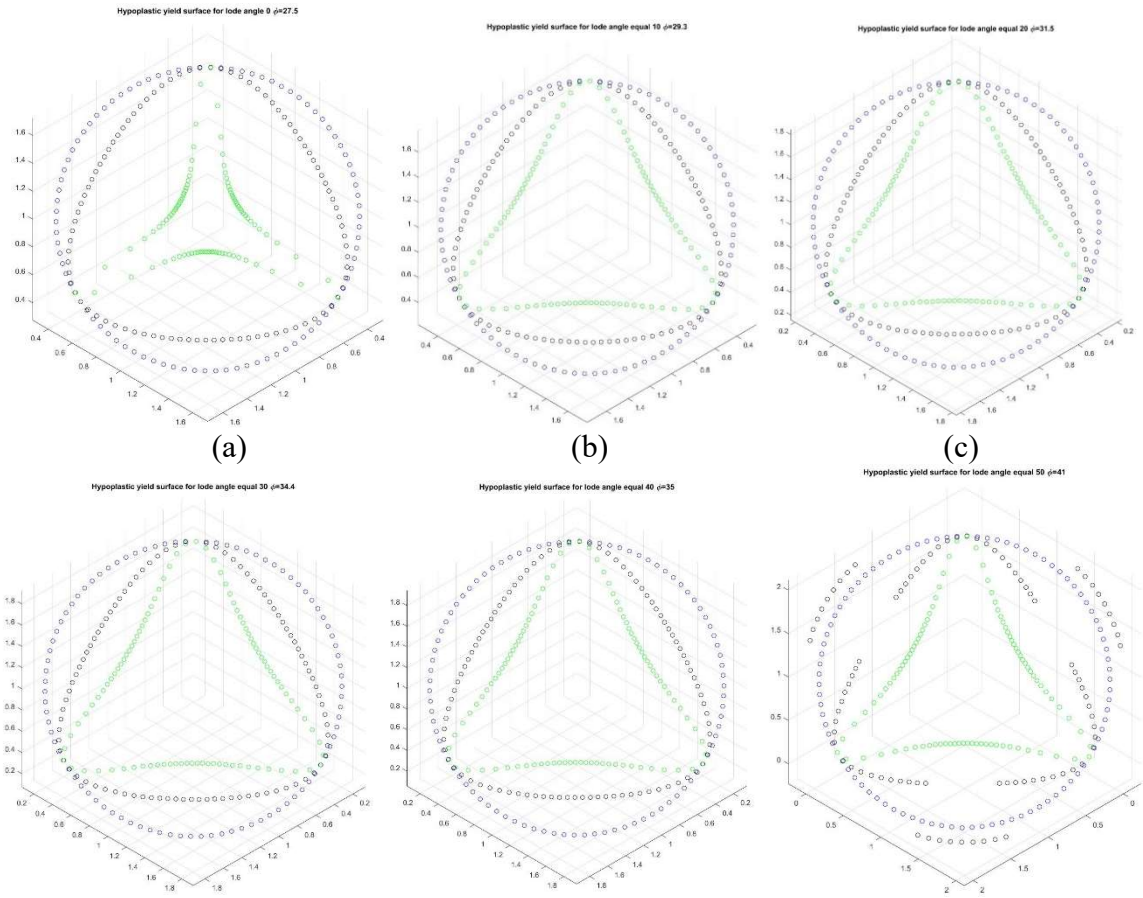

(d) (e) (f)

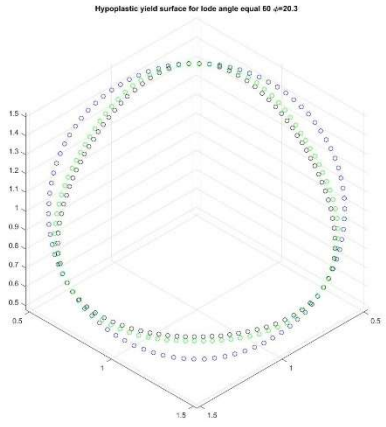

(g)

Figure 5-16 Hypoplastic yield surface in terms of original DEM true-triaxial test data for 125000 spherical poly-disperse spheres with different non-dimensional material parameters $C_i, i = 1,2,3,4$ under seven lode angle α condition (a) $\alpha = 0$ (b) $\alpha = 10$ (c) $\alpha = 20$ (d) $\alpha = 30$ (e) $\alpha = 40$ (f) $\alpha = 50$ (g) $\alpha = 60$ (calibrate with Lade-Duncan and Drucker-Prager yield surface at pure compression point)

It shows that the hypoplastic yield surfaces are calibrated Lade-Duncan and Drucker-Prager yield surface at pure compression point with $\varphi = 27.5,29.3,31.5,34.4,35,41,20.3$ (from a to g, respectively). Most of the yield surface in figure 5-16 such as the yield surface with case (b), (c), (d) and (e) keep the same shape. It coincides the result generated from figure 5-14&15, which is that the curves of parameter C in case (b) to (e) were stable. And in case (a), the shape of the hypoplastic yield surface is over-shrank and distorted, which is under-predict too much when it is compared with the Lade-Duncan yield surface. And the shape of the yield surface in figure 5-16f, the macro-scale friction angle φ is too large which will lead the shape of Lade-Duncan yield surface to be distorted. But it still not hard to figure out that the shape of the hypoplastic yield surface in that figure is similar as the one in (b) to (e).

Note that it is interesting that in the figure 5-16g, the shape of the hypoplastic yield surface match the Lade-Duncan yield surface well which was slightly over-predict (compared with Lade-Duncan yield surface).

Looking for the parameter C with the smoothed results from DEM true-triaxial test for 125000 spherical poly-disperse spheres, the hypoplastic yield surfaces are generated as follow (which are calibrated with Lade-Duncan and Drucker-Prager yield surface at pure compression point).

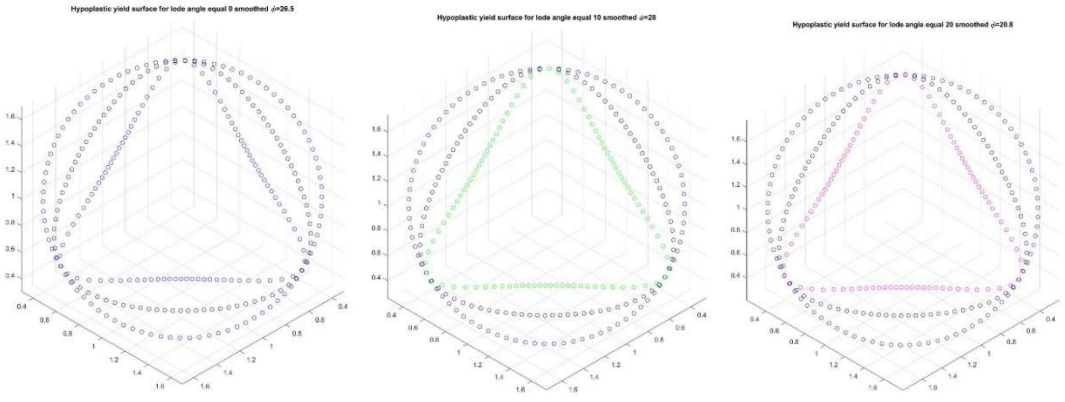

(a) (b) (c)

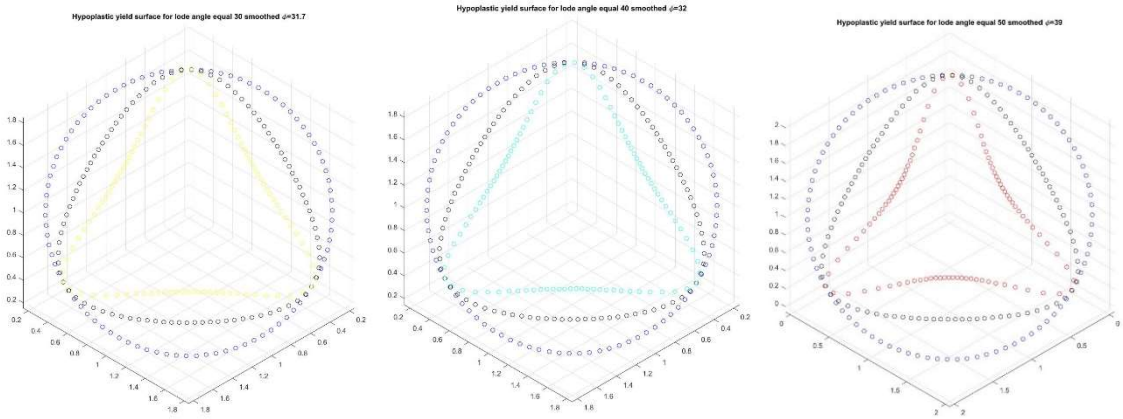

(d) (e) (f)

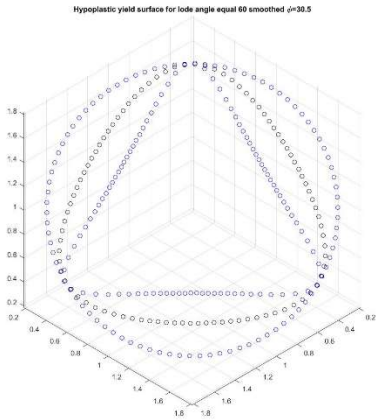

(g)

Figure 5-17 Hypoplastic yield surface in terms of smoothed DEM true-triaxial test data for 125000 spherical poly-disperse spheres with different non-dimensional material parameters $C_i, i = 1,2,3,4$ under seven lode angle α condition (a) $\alpha = 0$ (b) $\alpha = 10$ (c) $\alpha = 20$ (d) $\alpha = 30$ (e) $\alpha = 40$ (f) $\alpha = 50$ (g) $\alpha = 60$. (calibrate with Lade-Duncan and Drucker-Prager yield surface at pure compression point)

All seven hypoplastic yield surfaces are calibrated with Lade-Duncan and Drucker-Prager yield surface in pure compression with $\varphi = 26.5,28,29.8,31.7,32,39,30.5$, respectively. It can be observed that the shapes of the yield surface are uniform in figure 5-17 which is one of the most gratifying, even though the curve of the parameter C in figure 5-15 are not one hundred percent coincided. Note that, it is slightly under-predicted under the pure extension for the case (f) compared with another six samples. It may cause by the macro-scale friction angle φ for case (f), which is larger than any φ in seven hypoplastic yield surfaces. The same assumption is can be obtained from result in figure 5-16f with the raw DEM data. It shows that compared with the yield surface all the optimized hypoplastic yield surfaces are under-predict in pure-extension and even under-predict when it is compared with the Matsuoka-Nakai's. And it can be found that parameter C_1 and C_3 can be easily generated from both smoothed and original data and these two parameters do not impact the change of hypoplastic yield surface's shape due to the stable curve in figure 5-15.

In sum, fortunately, the shapes of hypoplastic yield surface for same specimen are coincided, which conform to the comprehension of hypoplastic model in general.

6 Conclusion and future work

6.1 Conclusion

The groups of the non-dimensional material parameters $C_i, i = 1,2,3,4$ with the input from the DEM true-triaxial test for both 3000-30000 mono-disperse spheres and 125000 spherical poly-disperse spheres, are obtained from the improved hypoplastic method in this paper. This method can be used to calculate the material parameter C which can be substituted into the hypoplastic constitutive model. The method introduced in chapter 3 has the ability to generate the parameter $C_i, i = 1,2,3,4$ which can be used to plot the yield surface matching with the Lade-Duncan, Matsuoka-Nakai, Mohr-Coulomb, Drucker-Prager etc. From them, the Lade-Duncan yield surface through the complicated mathematics calibration. It can only summarize the law of mathematics or so-called random probability which is hard to persuasive when these parameters C should be correlated with the material. In contrast, the improved method which is inspired by the Wu. W and Erich Bauer which was setting up two equations applied with initial condition for the triaxial test, can generate the attributive material parameter C. Due to the input of the improved method which is the stress and strain obtained from the true-triaxial test, the improved method is convinced to be material corresponded.

And it is different from the mentor (the idea from Wu. W and Erich Bauer), the complete true-triaxial test data is applied to generate parameter C. With the Moore-Penrose inverse method, hypoplastic constitutive model can be optimized to be the calculator for the parameter C. The totally inverse equation from original hypoplastic constitutive equation is successful match the size of the input which was the output from the DEM true-triaxial test for each specimen. Otherwise, the procedure for smoothing the DEM raw data

successfully eliminate most of the noisy data. And it is valid for the later process which is re-substituted the parameter C back into the hypoplastic constitutive equation. More than 150 cases of different specimen from DEM true-triaxial tests were discussed in this paper. Collaborating with the optimized inverse hypoplastic model for the parameter C study and the hypoplastic constitutive model, most of these cases were successfully produce the parameter C. And the least square method is applied to approximate the unique solution of the parameter $C_i, i = 1,2,3,4$. The concept of inverse the hypoplastic constitutive model is convinced to generate the actual and effective non-dimensional material parameters $C_i, i = 1,2,3,4$.

6.2 Future work

Right now, due to the noisy data, the result of the hypoplastic yield surface was not coincided with the Lade-Duncan yield surface which was considered as the most accurate one empirically, in pure extension. It is interested to further add different test data into the inverse hypoplastic parameter equation. Meanwhile, the more effective noisy eliminating procedure should be employed to smooth the stress path from the test. Otherwise, the input from the DEM true-triaxial can be added more options which was processed in [31]. Even though the hypoplastic parameter model can be processed well with the least square method for approximating the unique solution of the C, some more detailed algorithm can be applied on the model (e.g. GLS, RLS etc.).

Otherwise, as for hypoplastic theory, the constitutive equation introduced in this paper is just a drop in the ocean. It exists huge amount of different constitutive models which are corresponding with such as the nonidentical void ratio can generate more detailed

correlation between the hypoplastic yield surface and the Lade-Duncan yield surface. Due to the emphasis of this paper which is the parameter study, more work such as the response envelops especially useful tool in hypoplastic theory should be discussed. It should contain the ability for explaining the reason why Lade-Duncan yield surface, is such a good method, in the future.

BIBLIOGRAPHY

[1] Goddard, J. D., “Continuum modeling of Granular Media”, ASME, Vol. 66, 2014.

[2] Budiansky, B., and O’Connell, R., “Elastic Moduli of a Cracked Solid,” Int. J. Solids Struct., 12(2), pp. 81–97, 1976.

[3] Rao, K., and Nott, P., “An Introduction to Granular Flow (Cambridge Series in Chemical Engineering)”, Cambridge University, Cambridge, UK, 2008.

[4] Tejchman, J., “Shear Localization in Granular Bodies with Micro-polar Hypoplasticity (Springer Series in Geomechanics and Geoengineering)”, Springer, Berlin, 2008.

[5] Wu, W., Bauer, E., and Kolymbas, D., “Hypoplastic Constitutive Model with Critical State for Granular Materials,” Mech. Mater., 23(1), pp. 45–69, 1996.

[6] Kolymbas, D., ed., “Constitutive Modelling of Granular Materials” (Engineering Online Library), Springer-Verlag, Berlin, 2000.

[7] Lanier, J., Caillerie, D., Chambon, R., Viggiani, G., Besuelle, P., and Desrues, J., “A General Formulation of Hypoplasticity,” Int. J. Numer. Analyt. Meth. Geomech., 28(15), pp. 1461–1478, 2004.

[8] Muhunthan, B., and Sasiharan, N., “Fabric Dilatancy and the Plasticity Modeling of Granular Media,” Int. J. Numer. Analyt. Meth. Geomech., 36(9), pp. 1181–1193, 2012.

[9] Kolymbas, D., “Introduction to hypoplasticity”, CRC Press, 2000.

[10] Fleischmann, J. A., “Micromechanical Exploration of the Lade-Duncan Yield Surface by the Discrete Element Method,” March 27, 2018

[11] Wu, W. and Kolymbas, D., “Hypoplasticity then and now”, Constitutive Modelling of Granular Materials, 2000, Springer, pp. 57-106.

[12] Anne, Hoger, “The Material Time Derivative of Logarithmic Strain.”, Int. J. Solids structures Vol. 22, No9, pp. 1019-1032, 1986

[13] Truesdell C., and W. Noll, “The non-linear field theories of mechanics.”, Handbuch der Physik III/c. Springer-Verlag, 1965.

[14] Matsuoka, H. and Nakai, T. “Stress-deformation and Strength Characteristics of Soil Under Three Different Principal Stresses.”, Proc. JSCE 232, 1974, pp. 59–70.

[15] Lade, P.V. and Duncan, J.M. “Elastoplastic Stress-Strain Theory for Cohesionless Soil. J. Geotechnical.”, Engineering Division, 1975, 101, 1037–1053.

[16] Imole, O.I.; Kumar, N.; Magnanimo, V.; Luding, S. “Behavior of Frictionless Granular Assemblies Under Different Deformation Conditions.”, Hydrostatic and Shear, KONA Powder and Particle Journal 2013, 30, 84–108.

[17] Huang, X.; Hanley, K.J.; O'Sullivan, C.; Kwok, C.Y.; Wadee, M.A. "DEM analysis of the influence of the intermediate stress ratio on the critical-state behavior of granular materials.", Granular Matter 2014, 16, 641–655.

[18] J. Tejchman; W. Wu. "Numerical Simulation of Shear Band Formation with a Hypoplastic Constitutive Model.", Computers and Geotechnics, Vol. 18, No.1, pp.71-84, 1996.

[19] Fleischmann, J.A., Drugan, W.J. and Plesha, M.E. "Micromechanical Modeling of Yield in Isotropic Non-Cohesive Particulate Materials.", Geotechnical and Geological Engineering 2016, 34, 551–566.

[20] Fleischmann, J.A. "Micromechanics-Based Continuum Constitutive Modeling of Isotropic Non-Cohesive Particulate Materials, Informed and Validated by the Discrete Element Method.", PhD thesis, Department of Engineering Mechanics, University of Wisconsin–Madison, 2013.

[21] Fleischmann, J.A., Plesha, M.E., Drugan, W. J., "Determination of Yield Surfaces for Isotropic Non-Cohesive Particulate Materials by the Discrete Element Method.", Geotechnical and Geological Engineering 2014, 32, 1081–1100.

[22] Plimpton, S. "Fast Parallel Algorithms for Short Range Molecular Dynamics.", Journal of Computational Physics 1995, 117, 1–19.

[23] LAMMPS Website, http://lammps.sandia.gov. Accessed: 2018-3-27.

[24] Kloss, C., Goniva, C., Hager, A., Amberger, S. and Pirker, S., "Models, algorithms and validation for opensource DEM and CFD-DEM.", Progress in Computational Fluid Dynamics, An International Journal 2012, 12, 140–152.

[25] LIGGGHTS Website, http://www.cfdem.com/. Accessed: 2018-3-27.

[26] Ahrens, J., Geveci, B., Law, C. "ParaView: An End-User Tool for Large Data Visualization, Visualization Handbook", Elsevier, 2005.

[27] ParaView Website, http://paraview.org. Accessed: 2018-3-27.

[28] Fleischmann, J., "DEM-PM Contact Model with Multi-Step Tangential Contact Displacement History.", Technical Report TR-2015-06, Simulation-Based Engineering Laboratory, University of Wisconsin-Madison, 2015.

[29] Fleischmann, J., Serban, R., Negrut, D., Jayakumar, P., "On the Importance of Displacement History in Soft-Body Contact Models.", Journal of Computational and Nonlinear Dynamics 2016, 11, 044502–1–5.

[30] Fleischmann, J.A., Plesha, M.E., Drugan, W.J., "Quantitative Comparison of Two-Dimensional and Three-Dimensional Discrete Element Simulations of Nominally Two-Dimensional Shear Flow." International Journal of Geomechanics 2013, 13, 205–212.

[31] Wu. W and Erich Bauer, “A Simple Hypoplastic Constitutive Model for Sand.”, International Journal for Numerical and Analytical Method in Geomechanics, 1994, 18, 833-862.